ACS OMEGA

Open Access

http://pubs.acs.org/journal/acsodf

Article

Deterministic Models for Performance Analysis of Lignocellulosic Biomass Torrefaction

Abbas Azarpour, Sohrab Zendehboudi,* and Noori M. Cata Saady

Cite This: *ACS Omega* 2025, 10, 6470−6501

Read Online

ACCESS | Metrics & More | Article Recommendations

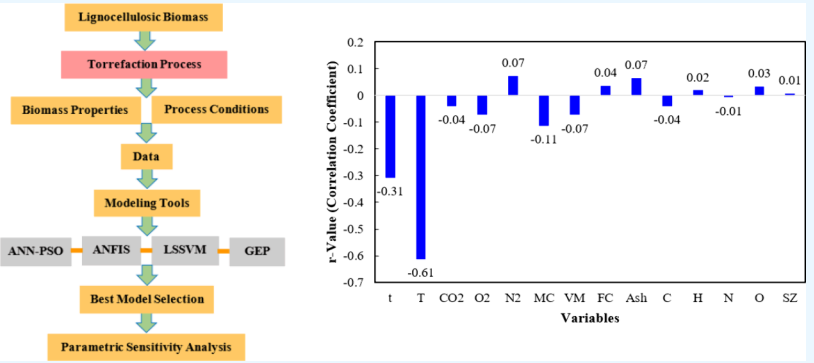

ABSTRACT: Energy plays a key role in the socioeconomic development of society, and most of its global demand is provided by conventional resources (e.g., fossil fuels). Utilizing renewable energy is significantly growing since it can meet global energy demand while minimizing the adverse impacts of carbon emissions on climate change. Biomass is an appealing option among the emerging alternatives (e.g., wind and solar). Torrefaction is a mild pyrolysis process, and this research aims to analyze the torrefaction process of lignocellulosic biomass. The methodology proposed involves employing hybrid models of artificial neural network-particle swarm optimization (ANN-PSO), adaptive neuro-fuzzy inference system (ANFIS), and coupled simulated annealing-least-squares support vector machine (CSA-LSSVM). In addition to the machine learning algorithms, a correlation is developed using gene expression programming (GEP) to interrelate the biomass properties, including moisture content, volatile matter, fixed carbon, ash, sample size, and the contents of oxygen, carbon, hydrogen, and nitrogen along with the process operating condition encompassing residence time, temperature, and the concentration of CO_2, O_2, and N_2 to the solid yield as the target variable. The results reveal that the CSA-LSSVM model has the highest accuracy, and the statistical metrics of the coefficient of determination (R^2), mean square error (MSE), and average absolute relative error percentage (AARE%) are 0.98, 0.00082, and 2.61%, respectively. The parametric sensitivity analysis demonstrates the residence time, temperature, and moisture content as the most influential variables, with temperature playing the most crucial role in the torrefaction process of lignocellulosic biomass. The findings and the developed models can be used to assess similar biomass torrefaction, providing the required knowledge for the modeling and optimization of the process. Hence, the bioenergy industry can be developed with optimal operating conditions, including cost and energy, and lessen the negative impacts of CO_2 emission.

1. INTRODUCTION

The significant increase in the world population and the growth of industries increased the energy demand; therefore, the sources of renewable energy, including solar, hydropower, wind, and bioenergy, have been regarded as potential substitutes for the fossil fuels.[1,2] Efficient use of energy needs to be critically considered in the advanced technologies.[3] The world's major energy sources are fossil fuels, supplying 80% of the world's energy.[4] Large utilization of fossil fuels in energy generation and industrial processes results in crucial environmental concerns, including acid rain, photochemical smoke, and large emissions of greenhouse gases (GHGs), especially CO_2. Today, it is commonly believed that CO_2 is the main cause of global warming.[5] The CO_2 concentration increased from 408.72 ppm in 2018 to 421.08 ppm in 2023.[6] The main purpose of using renewable energies is to limit the negative impact of burning fossil fuels on the environment.[1] Depletion of natural resources stipulates the need to find new sources of

Received: July 17, 2024
Revised: December 31, 2024
Accepted: January 27, 2025
Published: February 13, 2025

https://doi.org/10.1021/acsomega.4c06610
ACS Omega 2025, 10, 6470−6501

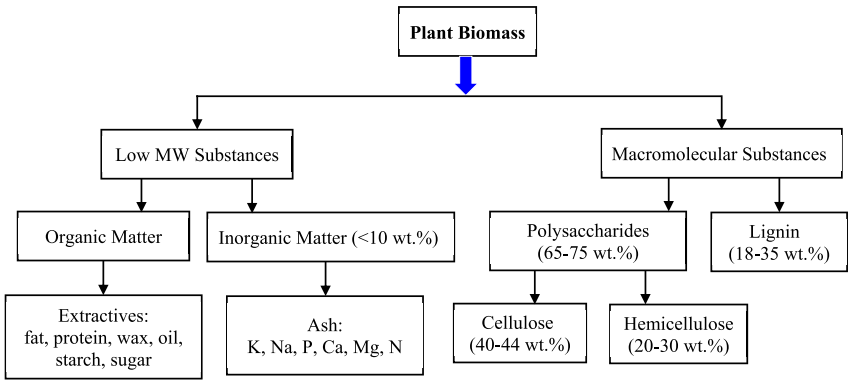

Figure 1. Biomass common chemical composition.[11] Adapted with permission from ref 11. Copyright 2020. Published by Elsevier Ltd.

energy. Therefore, substrates for the production of different chemicals and high-value-added materials need to be sought.[7] Biomass is the only abundant carbon resource available in nature.[8] Different biomass feedstocks, e.g., agricultural and forestry residues, wood processing residues, algae, and food wastes, can be utilized to produce biofuels and bio-based materials.[9,10] Figure 1 presents the plant biomass chemical composition.[11] Woody biomass is a carbon-neutral (renewable) fuel.[12,13] Utilizing wood energy as a replacement for fossil fuels can significantly reduce the emission of CO_2, which is a likely solution for mitigating global warming.[1] Lignocellulosic biomass is a main renewable energy source and is used via different thermochemical techniques, such as gasification, combustion, and pyrolysis. Nonetheless, compared to fossil fuels, raw biomass has several disadvantages. For example, its heating value is much less than that of fossil fuels due to its oxygen content and high moisture; therefore, it needs a higher space for transport and storage. Moreover, biological degradation can occur during extended periods. In addition, poor grindability causes difficulties for efficient combustion in large-scale furnaces.[14] Various chemical and biological methods can produce energy from lignocellulosic biomass, such as by converting it to combustible liquid and gaseous fuels, or burning it directly to generate heat/power.[4] Thermochemical processes are much faster than biochemical ones, requiring smaller reactor volume.[7]

Biomass should undergo a pretreatment process to conquer its disadvantages (e.g., large water content, poor grindability, weak moisture absorption, and low energy value) to increase its energy conversion efficiency.[15] Thermal conversion processes such as torrefaction, combustion, gasification, pyrolysis, and hydrothermal liquefaction are usual thermal technologies that can convert and upgrade biomass into different biofuels.[16] Torrefaction is a relatively more stable and energy-efficient process compared to other thermal pretreatment techniques, including hydrothermal carbonization and pyrolysis.[15] Torrefaction is a promising pretreatment process that allows large-scale biomass utilization.[17,18] Torrefaction, which is also known as soft pyrolysis, is a thermal treatment where the biomass is exposed to the temperature (200−300 °C) at a specified residence time, usually taking place in an inert atmosphere.[19,20] The inert torrefaction endothermic nature and absence of oxygen consume much energy.[21] During this process, hydroxyl (−OH) groups are removed, producing hydrophobic materials.[22] Furthermore, water and light volatiles encompassing most of the oxygen are removed from the biomass, and its fibrous structure is partly destroyed. This changes its property from hygroscopic to hydrophobic and improves the grinding characteristics. Moreover, biomass is converted into a carbonaceous material with outstanding properties, including high-calorie density, crushable, compressible, and low O/C and H/C ratios.[19] Wet torrefaction is the process of drying biomass by employing superheated steam at atmospheric pressure and then heating it to 220−250 °C in an O_2-free steam environment.[23] Biomass torrefaction can be carried out in different reactors, including fixed-bed, rotary drum, microwave, and fluidized-bed.[11] The torrefaction process produces solid biochar (or char), volatile gases, which can be separated into permanent gases (e.g., CO and CO_2) and liquid (condensable gases) (mainly consisting of moisture, lipids, and organics), considering room temperature as the reference temperature.[11] In processes such as pyrolysis and torrefaction, fluctuations in temperature endured by the particles of biomass owing to the reactor and operating conditions can reduce the energy yield, increase loss of biomass, and enhance heterogeneity of chemical species contained in the liquid product.[24] The operating conditions of the torrefaction process have been analyzed/assessed in numerous research works to enhance deoxidation and fixed carbon (FC), revealing the quality improvement affected by several parameters such as temperature, residence time, pressure, particle size, and pressurization mode.[25] The condensable gases resulting from the wood torrefaction process are a complex mixture containing more than one hundred oxygenated components (e.g., acids, alcohols, ketones, aldehydes, phenolic, furans, sugars, and guaiacols) diluted in water. A thermodynamic model combining the UNIQUAC model with chemical equilibria was developed to suggest various strategies of separation and purification (i.e., recovery of final products, such as glycolaldehyde, acetic acid, eugenol, and furfural). The model could provide acceptable results for the various binary systems for elevated composition ranges and pressures.[26] A kinetic model was proposed for the pre-torrefied lignocellulosic biomass pyrolysis to further elaborate the pyrolysis kinetics of raw biomass. A three-parallel first-order pyrolysis kinetic model was adapted to include severity factors encompassing the influence of torrefaction temperature and time on the biomass components of cellulose, hemicellulose, and lignin. It was reported that the employed model could accurately predict the differential thermogravimetry and pyrolysis yield of the pre-torrefied samples for different pyrolysis heating rates and torrefaction severities.[27] A symmetrical two-dimensional model was developed for the analysis of heat transfer inside large cylindrical biomass during

https://doi.org/10.1021/acsomega.4c06610
ACS Omega 2025, 10, 6470−6501

the torrefaction process. The model was used for the analysis of temperature distribution on the surface and within the core of cylindrical biomass with different sizes and the impact of length to diameter ratio of the biomass on the temperature distribution. It was verified that a cylindrical biomass sample of 5 cm length with the length to diameter ratio of two could be torrefied with a surface-core temperature difference of lower than 30 °C.[28] Addressing the quantification of biomass torrefaction pretreatment on the quality of the gases produced from the gasification with steam and steam-O_2 mixtures of non-woody biomass, a thermodynamic model was developed to predict the product gases composition as a function of steam to biomass ratio, temperature, biomass elemental composition, and equivalence ratio. It was revealed that the quality of the gases resulting from steam-O_2 gasification of untreated and torrefied biomass (i.e., tomato peels) did not vary significantly even though the torrefied biomass produced more CO and H_2 and less CO_2. In other words, although the torrefaction pretreatment had advantages of grinding, feeding, and storage, it provided a minimal improvement in the quality of product gas.[29] In another study, a one-dimensional mathematical model was utilized to simulate the performance of a torrefaction reactor incorporating direct heating and recirculation of the heat carrier, which includes exhaust gases from a gas piston unit and volatile torrefaction products. It was concluded that the mass loss degree during torrefaction is dependent on the temperature and the heat carrier mass flow rate at the reactor inlet.[26] A small-scale moving bed reactor used for the biomass torrefaction process was analyzed by using a mathematical model. The results revealed that the heat loss mechanism throughout the side wall is significant, and the axial thermal conduction has a critical role in the heat transfer within the reactor. Moreover, in the scale-up of the laboratory-scale reactor with the same torrefaction severity, there was an increase of 10−20% in the torrefied biomass mass yield owing to the decrease in the heat losses at a larger scale.[30] The optimization of the woody (first grade wood pellet) biomass torrefaction was carried out employing a one-dimensional simulation analysis. Lower heating value was significantly increased with increasing temperature and time.[31] The performance of a biomass torrefaction process was assessed by utilizing a one-dimensional model incorporating particle shrinkage, internal and external heat transfer, pyrolysis kinetics, and moisture evaporation. Considering three various kinetic models, it was found that the process is substantially influenced by boundary conditions, reaction rate, kinetics, and internal and external heat transfer.[32] Most of the studies on biomass torrefaction kinetics were implemented under isothermal conditions. A non-isothermal distributed activation energy model was developed to analyze the torrefaction kinetics of logging residue. The results showed that the main reactions taking place during torrefaction were carbonization and devolatilization of hemicellulose and partial decomposition of cellulose.[33] In a recent study, machine learning algorithms (e.g., artificial neural network (ANN), support vector machine (SVM), deep neural network, and gradient boosting machines) were used to predict the biochar properties from lignocellulosic biomass dry torrefaction considering the torrefaction operating conditions and biomass characteristics as the input variables.[20] Temperature was the most important factor impacting the higher heating value (HHV) and the yield of biochar.[20]

A main concern in lignocellulosic biomass is its inborn resistance of cellulose and hemicellulose in the conversion process of fermentable sugars production. Therefore, a pretreatment process is required to separate lignocellulosic biomass components, decrease its crystallinity, remove lignin, and provide the accessibility of the cellulose.[34] Lignocellulosic biomass conversion into end product (i.e., methane) is another challenge owing to its structure complexity.[35] Direct utilization of lignocellulosic biomass is usually demanding, owing to its poor thermochemical conversion performance and undesirable physicochemical properties (e.g., high moisture content, relatively low energy density, hygroscopic nature, and poor grindability). Torrefaction can enhance lignocellulosic biomass as a high quality solid biofuel, which can be employed for thermochemical conversion.[4] Torrefied biomass shows better grindability, higher energy content, and transport properties for injection (e.g., in a gasifier). Therefore, the process analysis of the torrefaction process is critical to remove the obstacles for improvement of the process, which can lead to the reduced operating cost of biofuel production and increased energy efficiency of the fuel. In this study, lignocellulosic biomass is analyzed using hybrid machine learning techniques including ANN-PSO, ANFIS, and CSA-LSSVM. Since the process evaluation can be better addressed using the mathematical measures, an equation reflecting the interrelation of the torrefaction process parameters is developed using GEP. Moreover, the parametric sensitivity analysis is carried out to determine the degree of impact of the crucial operating parameters on the process performance. Finally, the obtained results are discussed to better understand the process and to suggest practical suggestions for the relevant process industries.

2. THEORY AND BACKGROUND

This part encompasses the literature review on biomass torrefaction, including the reaction kinetics, first-principles model (FPM) development, and machine learning (ML) approaches. Moreover, the biomass torrefaction process is detailed, with a focus on the approaches employed to improve the process. Soft computing approaches (e.g., machine learning) are robust options for phenomenological, thermodynamic, and traditional modeling methods. These approaches have advantages including noise reduction potential, high flexibility, and high accuracy.[36] Recently, deterministic intelligent methods (e.g., LSSVM) have been extensively employed to accurately estimate the target parameters of convoluted systems based on pattern recognition.[37]

2.1. Literature Review. Many studies have been carried out on the torrefaction process. Different techniques, including FPM and ML algorithms, have been used to analyze the process to improve it in terms of cost and energy efficiency. This section summarizes these studies with a focus on the FPM and ML approaches.

Multiscale (e.g., reactor and particle) models of a torrefaction process need the quantification of the chemical and physical properties of the products of torrefaction to scrutinize the energy balance of the process. At the reactor scale, the heat of torrefaction might perform as a sink or local source of thermal energy; therefore, the profiles of conversion and temperature are significantly affected. Moreover, the chemical reaction and heat transfer phenomena are linked by the crucial mechanism of heat release at the particle scale. In addition, the solid physical properties (e.g., density, specific heat, and conductivity) and the particle temperature are interconnected, which determine the rate of heat diffusion through the particle. Then, accurate thermochemical and

https://doi.org/10.1021/acsomega.4c06610
ACS Omega 2025, 10, 6470−6501

kinetic models are required to describe the evolution of these properties. At the reactor scale, a correct calculation of the reaction enthalpy is required for process design and control. For instance, runaway thermal reactions can occur due to the process conditions that result in excessive heat release.[38] Assessment of kinetics and mechanisms of thermochemical conversion of biomass is vital for obtaining important knowledge that can be used to optimize parameters and design thermochemical reactors.[39] Several kinetic models have been developed for biomass torrefaction under a dry inert atmosphere. Most of these models are pseudomechanistic, where one or several pseudoreactions are considered for biomass torrefaction modeling. In a study, separate distributed activation energy models were developed for each of the cellulose, hemicellulose, and lignin lumps by observing their rates of thermal decomposition versus time in a torrefaction medium employing a thermogravimetric analyzer (TGA). It was concluded that the energy density of aspen and birch improved by reducing their hydrogen and oxygen content with reference to carbon in the solid residue.[40] Moreover, torrefaction decreased the equilibrium moisture content of aspen and birch and their main components (i.e., lignin, xylan, and cellulose) by 30−40%.[40] A feed-forward artificial neural network (ANN) was developed to predict the permeate flux in terms of total solid concentration and the filtration time in biomass leachate treatment and nutrient recovery. It was concluded that permeate flux is significant at the filtration beginning, which depends on the initial total solid concentration in the leachate.[41] A model was developed for the performance analysis of a torrefaction process considering gaseous and solid products' mass and energy balances.[18] The structure of the model was based on a C−H−O ternary diagram and the description of solid products in terms of composition, yield, and heating value. It was stated that the discussion of endo-exothermicity of the torrefaction reaction is not appropriate in the field of process integration since the process of torrefaction is always endothermic if the reaction heat and the sensible heat are considered in a steady state regime.[18] The impacts of wet torrefaction (WT) operating conditions (temperature and residence time) on the thermal decomposition in nitrogen and pyrolysis kinetics of woody biomass were investigated considering a three-pseudocomponent *n*th-order model. It was found that WT enhanced the pyrolysis peak height but reduced the amount of volatiles released during the process. Moreover, intense WT conditions (e.g., 30 min and 225 °C) reduced the pyrolysis rate because of the fast cellulose decomposition.[42] A phenomenological transient 2-D model was developed for the torrefaction process of large biomass particles considering mass and energy balances incorporated with a two-step biomass decomposition kinetic model (i.e., simultaneous production of solid and vapor from biomass and volatiles decomposition into gases and secondary char).[43] The results of the model revealed that the particle maximum internal pressure increased as a function of temperature and their size. This increase can improve the secondary reactions and char formation but might destroy the material if it surpasses its strength limits. Moreover, a smaller conversion was achieved at a certain residence time when the particle size increased due to the slower heat conduction into the particle.[43] In another modeling study, a mechanistic model of torrefaction was developed for a two-stage rotary reactor. The model includes mass and energy balances for each phase considering a kinetic model, which regards the biomass progressive decomposition into volatiles and char released from the biomass coupled to the balances. The model verified that the torrefaction process improved biomass properties such as high FC, large higher heating value (HHV), and low volatile matter (VM), which indicates a higher reactivity.[44] Performance of a biomass torrefaction unit, including a reactor, a dryer, two heat exchangers, and a combustor, was simulated in terms of mass and energy yields, volatiles, torrefied biomass compositions, process heat requirement, thermal efficiency, and CO_2 emissions. The simulation revealed that the temperature and moisture content greatly affected the CO_2 emission. The moisture content had a higher impact on the thermal efficiency than the residence time and temperature.[45] An experimental study examined the impact of the solid bed height, particle size, temperature, heating rate, and residence time on the formation and distribution of products in the torrefaction process of empty fruit bunches and mesocarp fiber from oil palm species. The results indicated that the temperature was the most influential parameter on the mass yield of the solid product. Moreover, the increase in the residence time reduced the mass yield of solid product for empty fruit bunches and fiber.[46] The pyrolysis kinetics and performance of the torrefied biomasses (i.e., rice straw and pine sawdust) were examined using the distributed activation energy model method and Friedman and Flynn−Wall−Ozawa technique employing a unique gas-pressurized torrefaction process for the improvement of their thermochemical properties.[47] The study signified that the thermal degradation of various components of the biomasses with increasing temperature led to fluctuations in the activation energy with the degree of conversion. At larger conversion amounts, the activation values of the gas-pressurized torrefied biomasses increased, and they were higher than the values of raw and atmospheric-pressure torrefied biomass for rice straw and larger than the value of raw biomass for pine sawdust.[47] The torrefaction kinetics of beech wood was investigated employing thermogravimetric analysis (TGA) at 220, 250, and 280 °C. The results signified that the *n*th-order model was more accurate that the first-order model, and it could be used for the appropriate analysis of the beech wood torrefaction.[48] In another study, a kinetic model was proposed to estimate the solid mass loss in torrefaction as a function of temperature, time, biomass type, and key macromolecular composition (i.e., cellulose, hemicellulose, and lignin). It was concluded that modeling the biomass torrefaction through the extracted macromolecular compounds was a more accurate strategy compared with employing commercial compounds. Moreover, the biomass performance in the torrefaction process depended on the biomass type.[49] The impacts of torrefaction on the characteristics of the biomass pyrolysis such as kinetics and volatile amounts were investigated to gain more understanding on the torrefied biomass pyrolysis, which could be employed for the design of the thermochemical conversion operation employing torrefied feedstocks. Increase in the severity of the torrefaction resulted in the reduction of either exothermic or endothermic impacts, and lower specific volatile was produced at the higher torrefaction degree.[50] In another study, a torrefaction model was established to estimate the fundamental properties of torrefied biomass (e.g., mass and energy yields). As the preliminary analysis, the simulation was carried out on the whole torrefaction stage (i.e., 200−300 °C) using a linear fitting method. In order to achieve a more accurate model, the model was developed using a two-phase torrefaction process

https://doi.org/10.1021/acsomega.4c06610
ACS Omega 2025, 10, 6470−6501

Table 1. Studies Carried out on Biomass Torrefaction Using ML Techniques

Process/Feedstock	ML Model	Parameters[a]	Sample Size	Findings	Reference
LB (agricultural residues, forestry residues, and energy crops)	Lss, NRR, KRR, DT, AdB, GTB, FRT, ERT, k-NN, SVM	**IP**: MC, VM, FC, ash, C, H, N, O, SZ, t, T, C_{N2}, C_{CO2}, C_{O2}	800	• GTB has the best prediction accuracy.	Onsree et al.[55]
		OP: SY		• T, t, C_{O2}, VM, C, and O have the highest impact on the model prediction.	
Raw LB	ANN	**IP**: T, t, FC, VM, ash	284	• The accuracy of ANN prediction is acceptable.	Kartal et al.[56]
		OP: Chemical exergy		• The MAPE value for both training and testing phases is less than 4%.	
Chlamydomonas sp., Chlorella sorokiniana CY1, *Chlorella vulgaris* ESP31, Arthrospira platensis, spent coffee grounds, and Chinese medicine residue	ANN, MARS	**IP**: type of feedstock, T, t	1626	• Artificial intelligence (AI) and MARS techniques satisfactorily predicted the TSI.	Chen et al.[57]
		OP: TSI		• MARS analysis implied that T has a crucial impact on TSI.	
LB (agricultural and forestry)	PSO-SVM, MLP, RF	**IP**: FC, VM, T, t, O/C, H/C	300	• PSO-SVM with a cubic kernel function has the best accuracy.	García Nieto et al.[58]
		OP: HHV		• VM has the most significant effect on the HHV prediction.	
Raw biomass	SVM-SA, MARS, RF	**IP**: FC, VM, T, t, O/C, H/C	300	• SVM-SA has the highest accuracy to predict HHV.	Nieto et al.[59]
		OP: HHV		• FC is the most important parameter to predict HHV.	
Various biomass feedstock (e.g., agricultural and forestry residues, energy crops, leaves, sewage sludge, and fruit wastes)	GA-BPNN	**IP**: MC, FC, VM, T, t	497	• GA-BPNN performed very well.	Liu et al.[60]
		OP: O/C, H/C, FR, HHV, SY, EY		• The model can be applied to biomass.	
Various biomass feedstock (e.g., agricultural residues, hardwood, softwood, energy crops, herbaceous biomass, and fruit shells)	ANN, ANFIS	**IP**: T, t, FC, VM, ash	448	• ANN prediction is better than that of ANFIS.	Kartal et al.[61]
		OP: C, H, O, HHV		• The model can predict the properties of torrefied biomass from any raw biomass and operating conditions.	
LB (agricultural residues, forestry residues, and energy crops)	GTB, RF, SVM	**IP**: T, t, C_{N2}, C_{CO2}, C_{O2}, SZ, SM, FR, VM, FC, ash, N, S, H/C, O/C, Hm, Ce, Lg	800	• GTB has the greatest performance.	Onsree et al.[62]
		OP: SY, HHV		• Operating conditions have the highest impact on the process performance.	
SDR (feedstock), Chlorella sp. GD, *Chlorella vulgaris* ESP-31 and FSP-E, and macroalga *Eucheuma denticulatum* (for ML training)	MARS, ANN, DT	**IP**: feedstock, classification, MC, ash, VM, FC, C, H, N, O, T, t, C_{H2SO4}	49	• ANN has the highest performance/predictability.	Chen et al.[63]
		OP: $C_{glucose}$		• The order of parameters significance for $C_{glucose}$ is C_{H2SO4}, t, and T.	
Various biomass feedstock (e.g., agricultural residues, forestry residues, energy crops, leaves, sewage sludge, and fruit wastes)	RF	**IP**: MC, VM, FC, ash, C, H, O, N, T, t	515	• The model has an outstanding prediction capability ($R^2 > 0.93$).	Liu et al.[64]
		OP: HHV, FR, H/C, O/C, N		• T is the most influential parameter for H/C, O/C, FR, and HHV.	

[a]LB: lignocellulosic biomass; Lss: lasso; NRR: normal ridge regression; KRR: kernel ridge regression; DT: decision tree; AdB: AdaBoost; GTB: gradient tree boosting; FRT: forests of randomized trees; ERT: extremely randomized trees; k-NN: k-nearest neighbors; SVM: support vector machine; GTB: gradient tree boosting; T: temperature; t: time; C_i: component concentration; C: carbon; VM: volatile matter; O: oxygen; ANN: artificial neural network; MAPE: mean absolute percentage error; MARS: multivariable adaptive regression splines; TSI: torrefaction severity index; PSO: particle swarm optimization; MLP: multilayer perceptron; RF: random forest; HHV: higher heating value; SA: simulated annealing; GA-BPNN: genetic algorithm-back-propagation neural network; ANFIS: adaptive neuro-fuzzy inference system; DT: decision tree; IP: input parameter; MC: moisture content; VM: volatile matter; FC: fixed carbon; C: concentration; OP: output parameter; HHV: higher heating value; FR: fuel ratio; SY: solid yield; EY: energy yield; SM: solid mass; Hm: hemicellulose content; Ce: cellulose content; Lg: lignin content.

https://doi.org/10.1021/acsomega.4c06610
ACS Omega 2025, 10, 6470−6501

Table 2. Torrefaction Process Reactions[11] [a]

Type of Reaction	Reaction	$\Delta H_{r298}\left(\frac{kJ}{mol}\right)$	Reaction Temp (°C)	Likelihood
	Biomass Drying			
Unbound moisture	Primary: $H_2O_{(l)} \rightarrow H_2O_{(g)}$	44.0	100−105	High
	Biomass Torrefaction			
Torrefaction	**Primary: Biomass$_{(s)}$ → Biochar$_{(s)}$ → Torrefaction gasses$_{(g)}$**	**Varies with biomass**	**200−300**	**High**
H_2O	Secondary: $H_{2(g)} + \frac{1}{2}O_{2(g)} \rightarrow H_2O_{(g)}$	−241.8	160−300	Low
CO_2	Secondary: $C_{(s)} + O_{2(g)} \rightarrow CO_{2(g)}$	−393.5	160−300	Low
CO_2	Secondary: $CO_{(s)} + \frac{1}{2}O_{2(g)} \rightarrow CO_{2(g)}$	−283.0	160−300	Low
CO	Secondary: $2C_{(s)} + CO_{2(g)} + H_2O_{(g)} \rightarrow 3CO_{(g)} + H_{2(g)}$	101.4	200−300	Low
CH_3COOH	Secondary: $2C_{(s)} + 2H_{2(g)} + O_{2(g)} \rightarrow CH_3COOH_{(g)}$	−432.8	200−300	Low
CH_2O_2	Secondary: $C_{(s)} + H_{2(g)} + O_{2(g)} \rightarrow HCOOH_{(g)}$	−378.6	200−300	Low
CH_3OH	Secondary: $C_{(s)} + 2H_{2(g)} + \frac{1}{2}O_{2(g)} \rightarrow CH_3OH_{(g)}$	−200.0	200−300	Low
$C_3H_6O_3$	Secondary: $3C_{(s)} + 3H_{2(g)} + \frac{3}{2}O_{2(g)} \rightarrow CH_3CH(OH)COOH_{(g)}$	−599.6	200−300	Low
$C_5H_4O_2$	Secondary: $5C_{(s)} + 2H_{2(g)} + O_{2(g)} \rightarrow C_4H_3OCHO_{(g)}$	−151.0	200−300	Low
$C_3H_6O_2$	Secondary: $3C_{(s)} + 3H_{2(g)} + O_{2(g)} \rightarrow C_3H_6O_{2(g)}$	−366.0	200−300	Low

[a]Adapted with permission from ref 11. Copyright 2020. Published by Elsevier Ltd.

including a mild stage (200−250 °C) and severe phase (250−300 °C) employing a quadratic equation. The results obtained from the torrefaction process completed on three biomasses (i.e., woody (Chinese fir), herbaceous (corn stalk), and shell-like (palm kernel)) revealed that the torrefaction pretreatment could significantly improve the low-grade fuels energy density.[51] Least square support vector machine (LSSVM) and extra trees machine learning algorithms were employed to predict cetane number, which is used to characterize fuel self-ignition ability. It was reported that the models have an acceptable accuracy to predict cetane number, and they could be used for biodiesel applications.[52] Oxygen-lean torrefaction can efficiently decrease the complexity and cost of inert torrefaction. Non-isothermal measurements were performed using a model-fitting kinetics method to understand the basics of oxidative and inert torrefaction processes. This analysis' results were employed to develop a two-step first-order kinetics model to describe oxidative and inert isothermal torrefaction. The results showed that an extra reaction should have been considered (three-step mechanism) when there was a high residence time in the torrefaction reactor at high temperatures.[21] Different machine learning algorithms (e.g., Gradient Boosting Regressor and Multilayer Perceptron) were employed to predict the CO_2 capture capacities by biomass waste.[53] The sensitivity analysis confirmed that temperature was the most important parameter in the process of CO_2 adsorption.[53] In a recent study, a novel kinetic model for torrefied biomass pyrolysis was developed from a three-parallel reaction model of raw biomass. The model considered the three structural changes caused by torrefaction (i.e., residual lignocellulosic composition, partial decomposition of weaker chemical bonds, and increase in the amount of FC). It was stated that, for the more accurate prediction of pyrolysis kinetics, at least two various torrefied samples were needed for a specified biomass to determine the FC profile.[14]

Many studies have been carried out to analyze different torrefaction processes by using ML algorithms. Commonly, seven ML algorithms have been used to model the torrefaction processes: artificial neural networks (ANNs), multivariable adaptive regression splines (MARS), tree family (e.g., decision tree (DT), gradient tree boosting (GTB), and random forest (RF)), adaptive neuro-fuzzy inference system (ANFIS), and support vector machine (SVM).[54] Table 1 includes the studies completed using ML techniques applied to the torrefaction processes.

The literature review shows that there have been limited studies carried out on torrefaction processes using ML algorithms. In this study, the torrefaction process of lignocellulosic biomass is scrutinized using hybrid intelligent models, including ANN-PSO, ANFIS, and CSA-LSSVM. The accuracy of the developed models is improved by optimizing the structures of the components involved in the models. Moreover, a mathematical expression is developed using Gene Expression Programming (GEP) encompassing the most significant parameters impacting the torrefaction process efficiency. The findings of this research can be used to develop more accurate modeling and optimize the torrefaction process, leading to a better process design, less cost of operation, and a more efficient process.

2.2. Torrefaction Process. Nowadays, the conventional thermochemical processes are combustion, gasification, pyrolysis, carbonization, liquefaction, and torrefaction. These processes' performance mainly depends on temperature and oxygen supply. Non-oxidative torrefaction is the dominant method employed for solid biomass pretreatment, which has great potential for industrial applications. Non-oxidative biomass torrefaction is performed via the five stages of initial heating, drying, postdrying, and intermediate heating, torrefaction, and cooling. Changes in the biomass properties resulting from torrefaction are attributed to the involved/coupled reaction mechanisms of dihydroxylation of hemi-

https://doi.org/10.1021/acsomega.4c06610
ACS Omega 2025, 10, 6470−6501

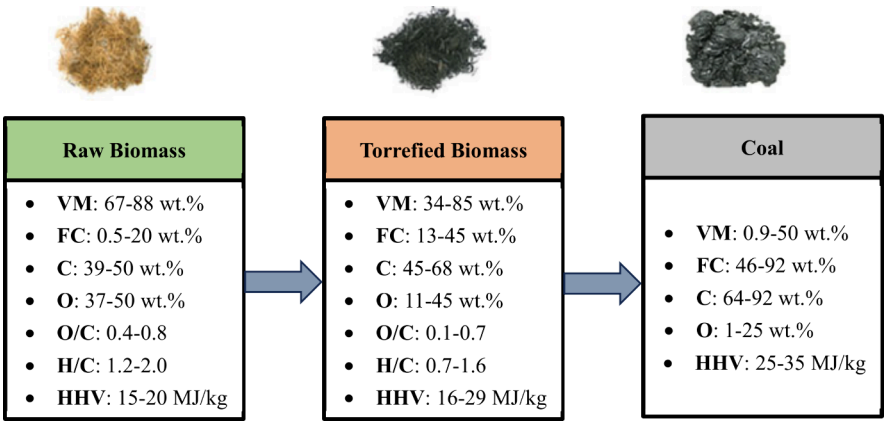

Figure 2. Comparative analysis of fuel characteristics: raw biomass, torrefied biomass, and coal.[65] Adapted from ref 65.

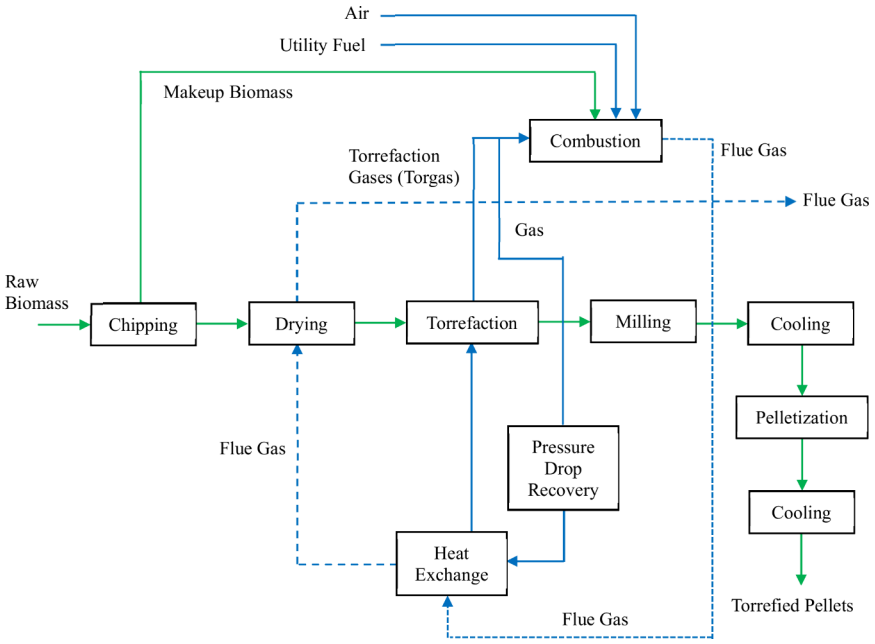

Figure 3. Simple layout of an integrated torrefaction plant.[74] Adapted from ref 74.

celluloses, decarboxylation and deacetylation of xylan-containing hemicellulose polymers, and demethoxylation and partial polymerization from lignin and cellulose.[65]

The purpose of torrefaction is to remove H, O, N, and S elements while leaving most of the C intact. In other words, gaseous products with C are not favorable since they reduce the carbon efficiency. Table 2 contains the chemical reactions that occur during torrefaction.[11] Table 2 illustrates the complexity of the torrefaction process by presenting a range of potential reactions. It is important to note that, while all of these reactions are theoretically possible, their likelihood and extent vary significantly under typical torrefaction conditions (200−300 °C in an inert atmosphere). The primary reactions in torrefaction are the devolatilization of hemicelluloses, dehydration, and decarboxylation. Secondary reactions, particularly those involving oxygen, are less likely in standard inert atmosphere torrefaction but may occur to a limited extent due to oxygen present in the biomass structure. The formation of various organic compounds is possible but generally limited. It is worth noting that our machine learning models can effectively analyze and predict torrefaction outcomes without explicitly modeling each of these reactions. This ability to generate useful predictions while bypassing the need to account for every possible reaction is a key strength of our connectionist modeling approach in handling complex processes such as torrefaction.[11] Fuel characteristics of raw biomass, torrefied biomass, and coal are illustrated in Figure 2.[65]

As a thermal pretreatment, the torrefaction process is a promising strategy for overcoming the pitfalls of biomass feedstocks and upgrading low-value lignocellulosic materials. However, the inadequate information on the existing plants performance and the process fundamental knowledge are the limiting factors for using this technology and its recognition as a strategic resource within the renewable energy supply chain.[66] Torrefaction as a thermal treatment process takes place in reducing atmosphere or probably moderately oxidative atmosphere (0−21% of oxygen); higher pressure can be used in certain cases[67] occurring over an appropriately high residence time (e.g., from several minutes to several hours).[68,69] By the combination of torrefaction and a following densification process, torrefied densified biomass is produced,

https://doi.org/10.1021/acsomega.4c06610
ACS Omega 2025, 10, 6470−6501

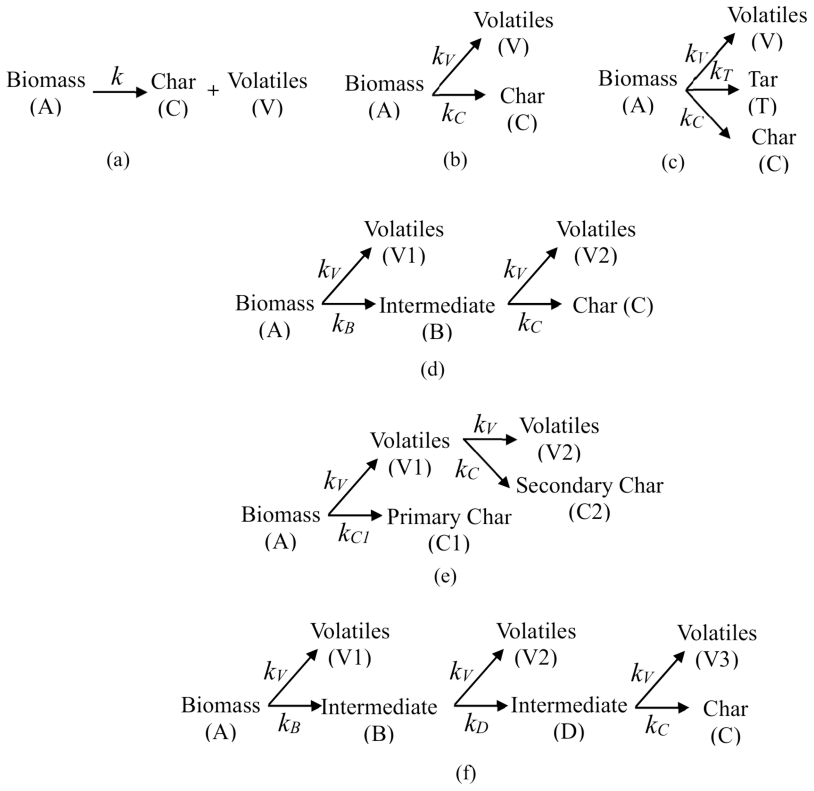

Figure 4. Various reaction mechanisms employed for biomass torrefaction: (a) one-step single reaction; (b) one-step two parallel reactions; (c) one-step three parallel reactions; (d) two-step with solid intermediates; (e) two-step with primary and secondary reactions; (f) three consecutive reactions.[67] Adapted with permission from ref 67. Copyright 2022. Published by Elsevier Ltd.

having superior characteristics compared to traditional pellets and untreated forest fuels.[70,71] The overall torrefaction process can be illustrated by the following relation:

$$\text{Raw Biomass} \xrightarrow{\text{Torrefaction}} \text{Torrefied Biomass} + \text{Condensable Volatiles} + \text{Gases} \quad (1)$$

The influence of temperature and residence time parameters on biomass torrefaction performance have been studied in numerous experimental studies.[72] The torrefied solid production requires thermal and electrical energy. In a stand-alone unit, the required heat is provided by burning volatiles and a utility fuel such as natural gas, emitting CO_2 and NO_x to the atmosphere. Recent research has revealed that torrefaction is the second largest contributor to the supply chain, with transportation from Canada to Europe sharing the largest portion. In a torrefaction plant integrated with a power plant, pressurized steam coming from turbine provides the process thermal energy, reducing the power plant power production capacity.[73]

Dry torrefaction is the thermal treatment of biomass in the temperature range 200−300 °C in the absence of oxygen; it liberates volatile organic compounds. This process is initially carried out via the devolatilization of hemicelluloses. Dehydration and decarboxylation reactions take place during the process of torrefaction. Even though 30 wt % of the biomass can be lost during the process, the torrefied product might contain 90% of the initial energy content. There has been a fast development of dry torrefaction technology to Technology Readiness Level 9 (e.g., Europe and North America). Figure 3 is a simple layout of an integrated torrefaction plant.[74] Wet torrefaction (WT) is usually carried out at 180−260 °C and up to 46 bar in a high-temperature compressed water or hydrothermal liquid medium under autogenic pressure.[75] WT, which is also called hydrothermal carbonization, is a process in which precursor materials are converted into hydrochar (a solid with coal-like specifications). Temperature is the key parameter in predicting the hydrochar quality succeeded by the residence time.[75] WT has some advantages compared to dry torrefaction. It applies to an extensive range of biomass types (e.g., sewage, sludge, and agricultural wastes (e.g., such as cow and swine manure[76])), it leads to high product quality (e.g., larger energy density and fixed carbon content), and it can efficiently remove inorganic elements.[77]

Several factors, such as the biomass composition and reactor operating conditions, influence the torrefaction. The product of different biomass torrefaction depends on temperature, residence time, chemical composition, particle size, heating rate, and the process environment. The composition of biomass consists of organic matter (e.g., hemicellulose, cellulose, lignin, and extractives) and inorganic matter (ash). The nature/source of biomass determines the proportional amounts of these constituents. Torrefaction starts from 200 °C with the hemicellulose decomposition; however, the biomass physicochemical characteristics vary more noticeably at temperatures greater than 250 °C. Temperature is the most critical parameter in the torrefaction process since it substantially influences the reaction rates and, therefore, the product composition and yields. Moreover, it impacts operational variables, including utility requirements and heat losses. The heating rate of biomass torrefaction depends on the feedstock particle size and the device heating rate. At low-temperature torrefaction, the warmup phase is comparatively

https://doi.org/10.1021/acsomega.4c06610
ACS Omega 2025, 10, 6470−6501

short; it is within 10−100 °C/min, similar to that usually applied in TGA equipment. Particle size can have various impacts in different reactors, or on various scales of the same reactor.[67] Consumption of energy for biomass grinding is affected by the variables of grinding machine, feed flow rate, and the material properties (e.g., initial particle size).[78] Large particles are favored at industrial scales since grinding raw biomass requires high energy (e.g., for wheat straws having a MC within the range of 4−7% and sieve dimensions of 3.2, 1.6, and 0.8 mm, the grinding specific energy was 41.0, 133.2, and 185.8 MJ/t, respectively).[78] Larger biomass particles have less surface area than smaller ones, thus decreasing the convective heat transfer rate. Moreover, larger particle sizes of biomass need more time to heat up owing to the larger mass and heat resistance. Increasing the biomass particle size improved the solid product yield and decreased the yield of noncondensable and condensable gases. In a torrefaction unit, the residence time is the period that solid feedstock resides in the zone within the range 200−300 °C. Typically, it is 10−60 min on average. The torrefaction reaction time is longer than those of gasification, combustion, and conventional pyrolysis to optimize char formation; therefore, a larger reactor volume is required. Even though it has been reported that temperature and residence time are independent variables, they are dependent variables in practical operations, particularly in a continuous mode of operation. In an oxidative torrefaction environment, a change in residence time has a comparatively higher effect on the reactor temperature than in an inert environment. Biomass torrefaction can be performed in different environments; however, the torrefaction process is mostly carried out in an inert atmosphere (absence of oxygen) to obtain larger yields of solid product.[67] Preferably, air or oxygen is introduced to an external combustor to harness energy from burning of volatiles released throughout the process without solids oxidation.[67] Biomass embodies several inorganic matters in addition to its essential lignocellulosic components. Alkali and alkaline earth metals can affect the composition and product distribution during pyrolysis, even at low temperatures. Metals, including potassium (K), sodium (Na), and manganese (Mn), which are organically bound in biomass, have positive impacts on its reactivity during torrefaction. Some catalysts (e.g., MgO and MgO−K_2CO_3) can increase the aromatic hydrocarbons and decrease the acids in the liquid yield of torrefaction.[67] Biomass thermal decomposition deals with a very convoluted set of reactions, which makes accurate formulation of kinetic models difficult. Knowledge of hemicellulose, cellulose, and lignin decomposition during the torrefaction process is critical to developing a substantial understanding of the process.

Figure 4 exhibits various reaction mechanisms employed for biomass torrefaction. These mechanisms differ in terms of intermediate steps, products, and the reactions that lead to varying reaction rate constants.[67]

3. MODEL DEVELOPMENT

Well-trained ML models can provide accurate predictions with a broader application range compared to other fast prediction techniques. Although ML's major weakness is its inability to extrapolate, this limitation can be mitigated by expanding the data set with new data points. Current ML models, such as SchNet and ChemProp, are readily available and user-friendly, requiring minimal experience to implement. The accessibility of ML has increased significantly with packages such as TensorFlow and scikit-learn and frameworks such as PyTorch and Keras. These tools allow researchers to implement deep learning with only a few lines of code, enabling them to focus on the physical meaning of their research rather than spending time developing complex computer models. However, ML techniques have some notable drawbacks. Their black-box nature makes them poor for explanatory studies despite their accuracy and speed. The lack of interpretability can make it challenging to design an appropriate ML model. In addition, determining the optimal number of training epochs can be difficult. While achieving high accuracy on training data is relatively straightforward for ML methods, the real challenge lies in obtaining high accuracy on unseen data. Models trained on small data sets are particularly prone to the influence of outliers. Furthermore, unlike human experts who can apply scientific knowledge and intuition to avoid nonsensical operations or experiments, ML techniques lack these inherent boundaries. This absence of built-in scientific constraints can potentially lead to unrealistic or inaccurate predictions.[79]

Models are developed to reflect the performance of a process of interest. Models can be physical, conceptual, and mathematical. Considering the degree of dependency on process knowledge versus process data, the models can be categorized into three classes: FPMs (white-box), hybrid models (gray-box), and data-driven models (black-box).[80] The process engineering field involves many dependent areas such as thermal, mechanical, bio, chemical, electrochemical, and systems-process engineering. Modeling the concealed process principles in a highly dimensional and complicated process involving numerous dependent variables, which is necessary for process design, control, optimization, and fault diagnosis, is very challenging. Experimentation and simulations, which involve many expensive manual interventions in modeling, are usually used to address this challenge. Therefore, finding and employing methods that reduce the utilization of experiments and simulations is necessary. Moreover, considerable amounts of data are produced in many fields due to the growing availability of sensors and networks, which are too complex and extensive for manual modeling. Steadily, the necessity for an automated way to model complicated systems has arisen. A promising solution for this challenge is the employment of Artificial intelligence (AI), particularly ML, in the modeling attempt.[81] ML algorithms can be used to evaluate the multivariable relationships in the biomass torrefaction process. ML is a subclass of AI that can learn and identify patterns from a data set without requiring explicit programming. It can access any type of data and derive knowledge outside of the main data set instead of just making predictions.[55]

Each thermal conversion method has varying outputs and various complexities; therefore, one ML approach might not be adequate for analyzing the process. The combination of ML algorithms with other ML models, advanced statistical tools, or metaheuristic optimization techniques has been verified to be a promising approach in the energy sector.[82] Hybrid models surpass the traditional models in terms of generalizability and accuracy but at the cost of enhanced computation effort.[82] Hybrid models provide benefits over strategies of other ML-based physical models including symbolic regression and sparse regression.[83] The advantages of hybrid models stem from the incorporation of fundamental knowledge (structuring knowledge or forming knowledge). The combination of structuring or forming knowledge can likely decrease the

https://doi.org/10.1021/acsomega.4c06610
ACS Omega 2025, 10, 6470−6501

number of data points needed for the characterization of the model application domain and increase the properties of extrapolation along certain domains.[83] The hybrid structure has two key benefits. Primarily, it does not utilize any approximation for the deep NN, and it is straightforward to apply and interpretable. Secondarily, the analysis of feature importance can be combined with the procedure of model structure selection, which indicates the feature relevance and provides a transparent model.[84] Therefore, the hybrid models of ANN-PSO, ANFIS, CSA-LSSVM, and GEP are used to analyze the torrefaction process system. ANN can search for solutions in a local region but are usually caught in a local minimum. PSO can search the global minimum and keep searching around it.[85] In an ANN-PSO model, PSO should decrease the errors of ANN by determining the optimal values for weights and biases of the model.[86] The ANFIS model incorporates the learning capability of NN and knowledge illustration of fuzzy logic (FL) employing linguistic expressions in an individual framework.[87] ANFIS has a significant performance in the estimation of nonlinear functions. When data points are not linear and distinct, ANFIS is more effective than other classifiers such as multiple linear regressions.[88] ANFIS can approximate any real continuous function to any degree of accuracy.[87] LSSVM is employed to increase the SVM modeling capabilities.[89] LSSVM can approximate any nonlinear function. For a conventional LSSVM model, it is difficult to gain acceptable results for data points with various trends.[90] The coupled simulated annealing (CSA) framework associated with LSSVM is structured to automatically start searching for the optimal parameters of the LSSVM model once the training phase begins. CSA is fast and can find the global minima.[91] GEP is an efficient mining algorithm, which produces models from data points with any prior knowledge.[92] GEP is an evolutionary computing algorithm that incorporates the robustness of genetic programming (GP) and simplicity of genetic algorithm (GA) by avoiding their drawbacks.[93] GEP can produce simpler models compared to GP, and it is faster than GP.[94]

3.1. Artificial Neural Network-Particle Swarm Optimization. An ANN is a cluster of neurons that behave as nodes in an interconnected network/system carrying out a target like the human brain's neural network.[95] The ANN utilizes a behavioral pattern to create a framework for modeling mechanisms. The structure of an ANN contains three layers, including input, hidden, and output layers, encompassing processing units called neurons, which are organized into several layers. The input layer received the input data. The output of a hidden layer (the middle layer), which receives data from the input layer, squashes the final output of the model. The hidden neurons use the weighted sum of the inputs to generate the intermediate output. The ANN model utilizes the activation function to calculate the outputs of the hidden and output neurons and employs the bias values to establish the output in addition to the weighted sum of inputs to the neuron. The network uses the bias values to set the output together with the weighted sum of the inputs to the neuron. The ANN modeling has two main parts: the network structure preparation and the weights of connections adjustment. Back-propagation (BP) is one of the most used training algorithms employed in ANN modeling/structure. The output of the ANN as the estimated value is compared with the observed value, and the error is minimized to determine the model weights. The weights and bias modification continue until the error values reach acceptable tolerance. However, the BP has a slow convergence, and a meta-heuristic optimization technique/algorithm should be used to overcome this weakness.[96] Swarm Intelligence (SI) is a cooperating mechanism built on a group of agents that accomplish a shared target by working together according to their system organization and behavior. The essence of the SI approach is the replication of the natural collective system behavior. Particle Swarm Optimization (PSO), Gravitational Search Algorithm, Gray Wolf Optimizer, and Cuckoo Search Algorithm are examples of SI algorithms which have high robustness, search efficiency, performance computing, simplicity, and a fast convergence rate.[97,98] These algorithms can optimize a large search space with a fixed-size population to solve various complicated design optimization problems.[98] The PSO algorithm is a population-based stochastic optimization technique.[99,100] It was introduced by Eberhart et al.[101] to analyze continuous nonlinear functions.[102] PSO performs based on the cooperative nature observed in bird flocks and fish shoals.[103] In this meta-heuristic technique/algorithm, every possible solution is viewed as a particle in a search space, and the particles create a swarm, exploring the entire search space together.[104] The best member of the population movement is learned, and a global best position is achieved based on this experience. The combination of ANN and PSO (ANN-PSO) significantly decreases the drawbacks of ANNs and increases the accuracy and efficiency of the technique. The weaknesses of the smart modeling approach include difficulty in initializing control parameters, inability to handle the swarm scattering problem, and a tendency to get trapped in local minima, leading to premature convergence.[99] In this hybrid approach, PSO is used to determine the ANN's initial weights, and they are updated until a converged solution is attained. Thereafter, the updated weights are considered/set as input ones to the ANN.[102] The first step of the optimization process is the particles' random distribution during search. The values of the personal best (p_{best}) and the global best (g_{best}) are the optimal solution that has a particle and the optimal solution determined by the swarm, respectively. Thus, p_{best} (cognitive component), g_{best} (social component), and the current speed of the particle are used to calculate the speed of the particle in the next step. The selection of both the cognitive component and the social component is random. Equation 2 represents the model:[86,105,106]

$$V_{id}^{k+1} = V_{id}^{k} + c_1 \times rand(0, 1) \times (p_{id} - x_{id}^{k}) + c_2 \times rand(0, 1) \times (p_{gd} - x_{id}^{k}) \quad (2)$$

where V_{id}^{k} and x_{id}^{k} denote the speed and the position of the i particle in the kth iteration in the dth dimension, respectively; V_{id}^{k+1} and x_{id}^{k+1} represent the ith particle's speed and position in the $(k+1)$th iteration in the dth dimension; p_{id} indicates the best location of the particle (p_{best}) in the dth dimension; p_{gd} symbolizes the best global position (g_{best}) in the dth dimension; c_1 and c_2 signify the identifying/cognitive parameter and the social parameter, respectively; and $rand(0,1)$ implies any numbers within the range of $[0, 1]$. The starting point/position of each solution is taken randomly, and the position of each solution is updated/optimized by utilizing eq 3:

$$x_{id}^{k+1} = x_{id}^{k} + V_{id}^{k+1} \quad (3)$$

https://doi.org/10.1021/acsomega.4c06610
ACS Omega 2025, 10, 6470−6501

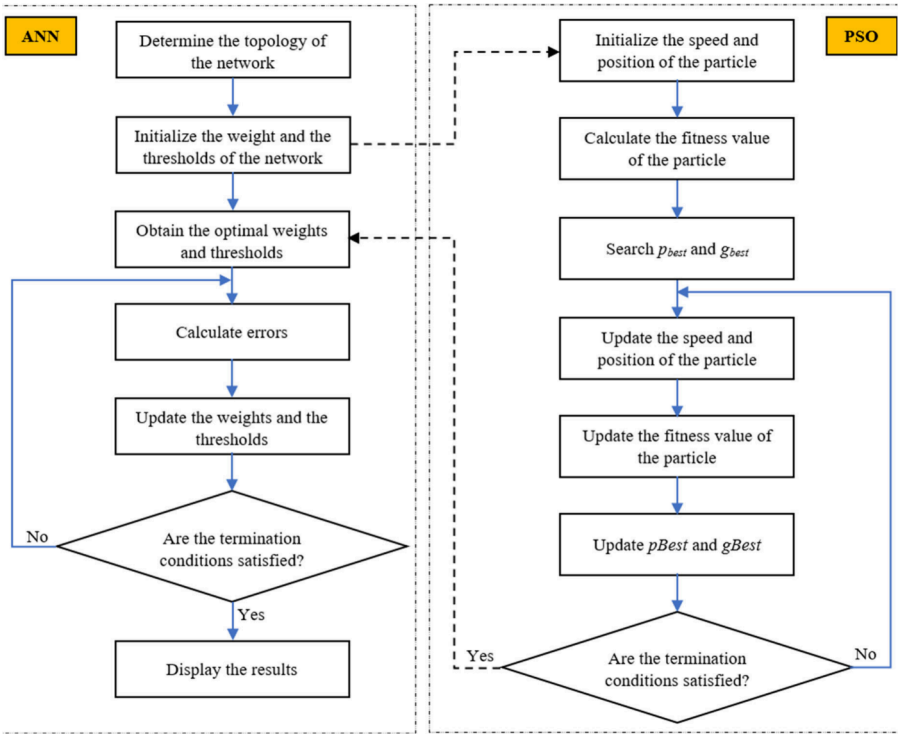

Figure 5. ANN-PSO computer algorithm.[107] Adapted from ref 107.

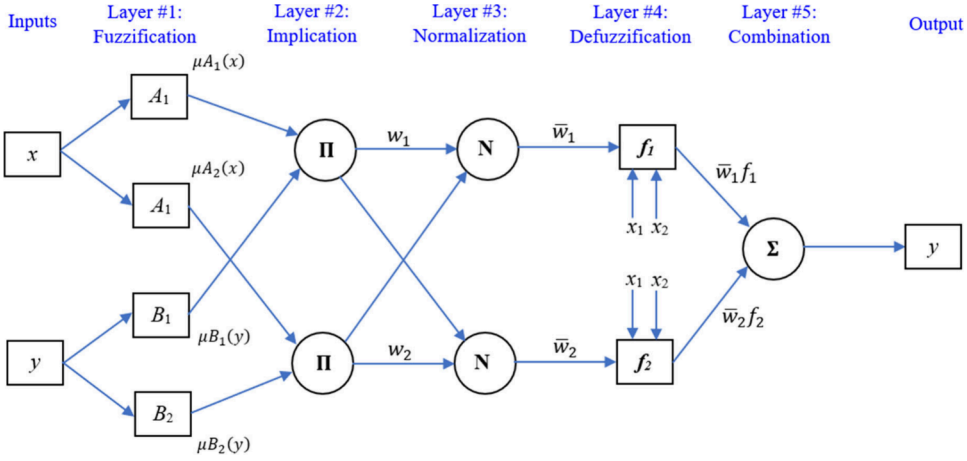

Figure 6. An ANFIS model with two inputs, first-order Sugeno FIS, and two rules.[107] Adapted from ref 107.

Figure 5 depicts the algorithm of the hybrid model of the ANN-PSO.

The performance/procedure of the ANN-PSO model is summarized below:[106,108]

- Use of the data set to train ANN
- Determination of the number of weights and biases in the ANN
- Optimization of the network training by the PSO algorithm through the following steps
- Determination of c_1, c_2, the algorithm's number of iterations, and the initial population of the PSO
- Calculation of the position and speed of each particle (the speed of each solution is equal to its starting position at the initialization step)
- Random selection of initial positions and starting speeds
- Determination of particle fitness function via decreasing the error produced by the ANN
- Calculation of a new position and speed by manipulating c_1 and c_2
- Comparison of local and global optimal values
- Organization of the particles and the attainment of an optimal solution
- Termination of the process if the maximum number of iterations is reached; otherwise, the error reduction goes on by the ANN
- When the optimal solution is achieved, the optimal weights and biases are fed/applied to the ANN

3.2. Adaptive Neuro-Fuzzy Inference System (ANFIS).

An artificial neural network (ANN) is a reliable approach for the analysis of complex problems (e.g., fluid flow, heat, and pattern recognition), as the quality of the computing tool is maintained.[109] ANFIS is a fuzzy-rule-based network that employs adaptive systems to foster the adaptation and learning process.[110] The key objective of the ANFIS is to optimize the

https://doi.org/10.1021/acsomega.4c06610
ACS Omega 2025, 10, 6470−6501

fuzzy inference system (FIS) parameters by utilizing input−output data sets via a learning algorithm.[110] The ANFIS technique combines ANN and fuzzy logic approaches, which can learn complex physical systems.[109,111] The ANFIS method benefits from ANN's learning ability and the fuzzy system's robust estimation capability.[112] The fuzzy logic approach mimics humans' decision-making that incorporates all the possibilities within the specific range of values.[113] Moreover, it is extensively employed in the decision-making processes, requiring expert knowledge.[113] The weaknesses of the ANFIS model could include high computational cost, the number and type of membership functions, a membership function location, and the problem of dimensionality.[114] In the structure of ANFIS, the nodes in the first layer and last layers indicate the input and output data, as the nodes in the hidden layers are characterized as membership functions (MFs) and rules.[110] The Sugeno model is extensively employed in the ANFIS structure due to its adaptability, interpretability, and high computational capability.[110] The ANFIS network is composed of five layers, as shown in Figure 6.

Figure 6 shows the nodes of the layers and their connections with the supposition of two inputs to the FIS, which are symbolized as x and y and a single output as f. In the ANFIS structure, two fuzzy IF−THEN rules are incorporated, obeying the Sugeno FIS as follows:[112,115]

Rule 1:

$$\text{if } x \text{ is } A_1 \text{ and } y \text{ is } B_1, \text{ then } f_1 = a_1x + b_1y + c_1 \tag{4}$$

Rule 2:

$$\text{if } x \text{ is } A_2 \text{ and } y \text{ is } B_2, \text{ then } f_2 = a_2x + b_2y + c_2 \tag{5}$$

where A_1, A_2, B_1, and B_2 are four input MFs for input parameters x and y. In this case, each input has two MFs. The values of a_i, b_i, and c_i are computed employing the least-squares error method. Each layer includes fuzzification, normalization, merge, and summarization. If μ_{A_i} and μ_{B_i} are the MFs of fuzzy sets A_i and B_i, $O_{i,1}$ is the output from the ith node of the first layer.[115,116]

Layer 1: Membership weights are generated for the fuzzy sets based on MF:[115,116]

$$O_{i,1} = \mu_{A_i}(x);\ i = 1, 2 \tag{6}$$

$$O_{i,2} = \mu_{B_i-2}(x);\ i = 3, 4 \tag{7}$$

where $O_{i,1}$ is the output from the ith node of the first layer.

Layer 2: Rules are generated by executing AND operator to the two entering membership weights:[115,116]

$$O_{i,2} = w_i = \mu_{A_i}(x) \times \mu_{B_i}(y) \tag{8}$$

Layer 3: The weight is normalized for the merge process:[115,116]

$$O_{i,3} = \overline{w}_i = \frac{w_i}{w_1 + w_2};\ i = 1, 2 \tag{9}$$

Layer 4: The output is computed by multiplying the entering normalized weight using the linear regression model:[115,116]

$$O_{i,4} = \overline{w}_i f_i = \overline{w}_i(a_ix + b_iy + c_i);\ i = 1, 2 \tag{10}$$

Layer 5: All the products are summarized from layer 4:[115,116]

$$O_{i,5} = \sum_{i=1}^{2} \overline{w}_i f_i = \frac{\sum_{i=1}^{2} w_i f_i}{\sum_{i=1}^{2} w_i} \tag{11}$$

3.3. Coupled Simulated Annealing-Least Squares Support Vector Machine (CSA-LSSVM). ANN-based techniques may have some drawbacks in the results regeneration since the network parameters are randomly initialized, and the variations of termination criteria may negatively affect the model's prediction quality. As an alternative, support vector machine (SVM) has been realized as a robust ML method, that works based on the nonlinear mapping of the data set to map input data into larger dimensional space.[117,118] Using optimization-based techniques improved the theoretical basis and developed practical data mining applications. An SVM algorithm is one of the most famous mathematical optimizations.[119,120] An SVM model is a powerful approach for supervised learning, which was formulated based on learning theory, and it is a proper method for data classification, regression analysis, and function approximation in multidimensional spaces.[121] In regression problems, SVM techniques are formulated and designed to solve a convex quadratic problem dealing with inequality constraints for locating and finding support vectors. However, significant computational obstacles due to the constrained optimization algorithms usually lead to time and memory limitations when SVM is applied in regression problems that encounter considerable experimental data. Moreover, SVM suffers from the uncertainty problem due to noise in data and process.[122] This technique is also inefficient in handling non-Gaussian noise and is vulnerable to outliers.[123] A modified version of SVM, called LSSVM, has been developed by Suykens et al.[124] to overcome the described drawbacks.[125] In an LSSVM model, equality constraints are used instead of inequality constraints, wherein the sum of squared error is employed as a cost function (CF), which is usually utilized in training classical NNs. Another advantage of an LSSVM approach in regression problems is its capability to use all sample data to develop the model.[121,126]

If x_i and y_i are the input vector and target output, respectively, in a training data set in the form of $\{(x_1, y_1), (x_2, y_2), ..., (x_N, y_N)\}$, eq 12 is used for the regression model:[127]

$$y = \langle w, \Phi(x)\rangle + b \tag{12}$$

where w introduces the weight factor, b is the bias term, $\Phi(x)$ refers to a nonlinear mapping function, and $\langle w, \Phi(x)\rangle$ denotes the scalar product of the w and $\Phi(x)$ vectors. The following CF is to be minimized to implement regression utilizing the LSSVM technique:[127,128]

$$\text{CF} = \frac{w^Tw}{2} + \frac{1}{2}\gamma \sum_{i=1}^{N} e_i^2 \tag{13}$$

where w^T introduces the transposed matrix of w, γ stands for the regularization constant, i represents each training data point, N denotes the number of training data points, and e_i refers to the regression error for each training data point.

The CF performance is conditional on the equality constraints:

$$y_i = \langle w, \Phi(x_i)\rangle + b + e_i;\ i = 1, 2, ..., N \tag{14}$$

The Lagrange function for this optimization problem has the following form:

https://doi.org/10.1021/acsomega.4c06610
ACS Omega 2025, 10, 6470−6501

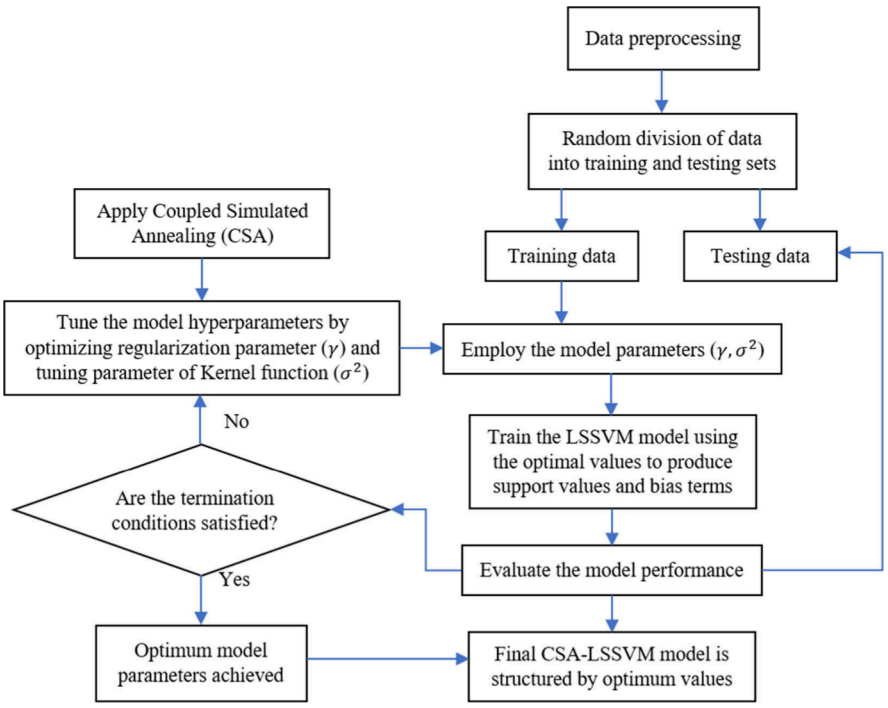

Figure 7. A layout of a CSA-LSSVM algorithm.[107] Adapted from ref 107.

$$L = \frac{1}{2}\|w\|^2 + \frac{1}{2}\gamma\sum_{i=1}^{N} e_i^2 - \sum_{i=1}^{N}\alpha_i\{\langle w, \Phi(x_i)\rangle + b + e_i - y_i\} \tag{15}$$

where α_i symbolizes the Lagrange multiplier. The following are the L equation partial differentiation with respect to w, b, e_i, and α_i:[89,127]

$$\frac{\partial L}{\partial w} = 0 \rightarrow w = \sum_{i=1}^{N}\alpha_i\Phi(x_i) \tag{16}$$

$$\frac{\partial L}{\partial b} = 0 \rightarrow \sum_{i=1}^{N}\alpha_i = 0 \tag{17}$$

$$\frac{\partial L}{\partial e_i} = 0 \rightarrow \alpha_i = \gamma e_i \tag{18}$$

$$\frac{\partial L}{\partial \alpha_i} = 0 \rightarrow \langle w, \Phi(x_i)\rangle + b + e_i - y_i = 0 \tag{19}$$

The following set of linear equations resulted from allowing $\alpha = [\alpha_1, ..., \alpha_N]^T$, $Y = [y_1, ..., y_N]^T$, $1_N = [1, ..., 1]^T$ and eliminating w and e:

$$\begin{bmatrix} 0 & 1_N^T \\ 1_N & \Omega + \gamma^{-1}I_N \end{bmatrix}\begin{bmatrix} b \\ \alpha \end{bmatrix} = \begin{bmatrix} 0 \\ Y \end{bmatrix} \tag{20}$$

where I_N is the $N \times N$ identity matrix and Ω is the kernel matrix expressed as:[91,127]

$$\Omega_{ij} = \Phi(x_i)^T\Phi(x_j) = K(x_i, x_j);\ i, j = 1, 2, ..., N \tag{21}$$

where $K(x_i, x_j)$ is the kernel function. Kernel functions can perform the ML techniques in multidimensional implicit feature spaces via applying the inner products between the images of all data pairs in the feature space, eliminating the requirement for calculating the coordinates of data points in the spaces. Different kernel functions such as spline, bspline, linear, polynomial, sigmoid, and radial basis functions (RBFs) can be utilized in the LSSVM approach. Polynomial and RBF are the broadly employed kernel functions as described below, respectively.[127,129]

$$K(x_i, x_j) = \left(1 + \frac{x_i^T x_j}{c}\right)^d \tag{22}$$

$$K(x_i, x_j) = \exp\left(\frac{-\|x_i - x_j\|^2}{\sigma^2}\right) \tag{23}$$

where b and c are constants and σ is the width of the RBF, which is used to control the ability of the regression. In this research, RBF is used as the kernel function. Therefore, to ensure good generalization and fast convergence, the values of σ and γ (regularization parameter) must be optimized.[127] In this study, a coupled simulated annealing (CSA) is hybridized with an LSSVM to determine the optimal values of the width of the RBF and the regularization parameters. Simulated annealing (SA) is a stochastic technique, usually employed for combinatorial optimization problems.[128] The SA was developed by Metropolis et al.[130] and was simplified by Kirkpatrick et al.[131] SA was developed to escape from local minima.[128] This method was inspired by the annealing process wherein a metal is heated to form a liquid phase and then cooled down gradually, thereby all crystal grains attaining the lowest inner energy eventually.[128] Like the annealing process, SA progressively converges to the optimal value/solution, ensuring the accomplishment of the global optimum while avoiding the local optimality.[128] CSA, which was invented by Xavier-de-Souza et al.,[132] presents a new version of acceptance probability functions that can be used for a group of optimizers.[133] The coupling is a function that contains the

https://doi.org/10.1021/acsomega.4c06610
ACS Omega 2025, 10, 6470−6501

costs of all individual SA processes.[128] A layout of the CSA-LSSVM is depicted in Figure 7.

3.4. Gene Expression Programming (GEP). Genetic programming (GP)-based modeling techniques are categorized as individual computational programming, which is a main group of soft computing approaches. GP models can analyze complicated and significantly nonlinear processes.[116,134] Gene expression programming (GEP) is a data-driven approach influenced by Darwin's idea of survival-of-the-fittest (and Mendel's genetic theory),[135] which heuristically evolves the parametric model until the error is decreased beyond a threshold.[136−138] In contrast to GP, which proposes only a single program, GEP incorporates several genes of programming for obtaining optimal solutions. Using GEP in the engineering area is advancing significantly compared to GP primarily due to the accuracy of its predictions.[116] The development of GEP was inspired by the genetic algorithm (GA) and GP, which Ferreira[139] invented to solve complicated problems. There are major differences between GA, GP, and GEP. Contrary to the GP, GEP can accomplish acceptable results more successfully in nonlinear and complex problems. Compared to GA, GEP can provide the desired results, expressing the relationships between nonlinear variables in different dimensions. GEP can function thoroughly in computational terms, particularly when coping with large-scale problems, which produces targeted results in a time-taking process.[140] However, the GEP model has some drawbacks, including the need for complex heuristics to obtain optimal results, the risk of overfitting, and significant computational challenges.[141] The GEP solution is assessed using expression trees (ETs). Each sub-ET comprises multiple chromosomes, represented as tree-like structures. A linking function—such as subtraction, addition, multiplication, or division—is used to connect the sub-ETs.[142,143] A fitness function, such as the root-mean-square error, is used to evaluate each output. The key components of the GEP are chromosomes, genes, and ETs. The GEP model is organized into ETs, which consist of several sub-ETs (genes). Each gene contains multiple chromosomes, which can be constant values, input variables, or functions. A gene is divided into a head and a tail: the head contains mathematical functions and terminal symbols, while the tail consists of terminal symbols, such as variables or constants, that adjust the equation in the model. The GEP's major operators are selection, mutation, transposition, and crossover, which is like GP, allowing the program to generate the next generation with better fitness scores.[142] The translation of information between chromosomes (genotype) and ETs (phenotype) is carried out flawlessly in the GEP, which makes modifications in readily manipulated elements (e.g., chromosomes) to truly replicate a genotype/phenotype relationship. Relating to the selection for fitness, the best-fitted ETs are selected for reproduction with their chromosomes' modification, comparable with the humans' reproduction.[144] Figure 8 shows the ETs for the following equation:

$$\sqrt{\frac{(a-d)}{(c+b)}} + \sin\left(\frac{c}{b}(1.7+a)\right) \tag{24}$$

GEP is employed in developing mathematical models and computer programs.[145] This study uses GEP to derive mathematical models by automatically applying different mathematical transformations to likely predictors and continually evolving the obtained model structures. The developed specified functions and the prediction capability of the models by GEP can be comparable to ML models, including random forest RF, ANNs, SVM, and kernel ridge regressions.[146] Figure 9 displays a simplified algorithm for the GEP model development.

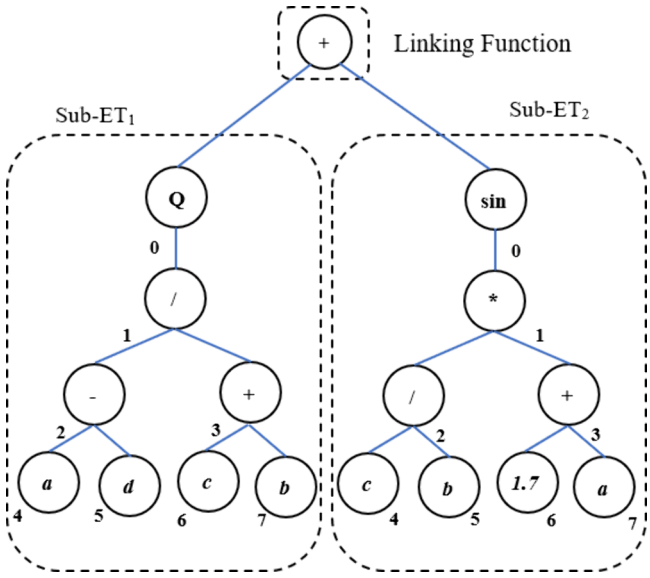

Figure 8. Phenotype expression tree for eq 24: root node (0), function nodes (1, 2, 3), and terminal nodes (4, 5, 6, 7).[107] Adapted from ref 107.

One of the most significant features of GEP is that it can produce mathematical formulas and correlations to forecast the performance of a typical process.[147] In the problem-solving procedure by GEP, a number of candidate solutions at each iteration are denoted as a chromosome, which is also called a genotype. The key variables and constants are positioned at the gene's head, while the tail holds only terminals. If the tail's length, the head's length, and the number of function's arguments are considered *tl*, *hl*, and *nf*, respectively, the following relation can be written:

$$tl = hl(nf - 1) + 1 \tag{25}$$

It is considered that the function $f^{\text{guess}} = f(x, y)$ completely fits a data set of m elements, which can be exemplified by x_p, y_p, and f_p, where $p = 1, 2, 3, ..., M$ are training data. The primary goal of GEP modeling is to explore all function domains to arrive at the best solution to fit the data. Therefore, the following equation can be introduced as a fitness function:

$$F(f^{\text{guess}}) = \frac{1}{M}\sum_{p=1}^{M}\frac{\|f^{\text{guess}}(x_p, y_p) - f_p\|}{\|f_p\|} \tag{26}$$

where the comparable distance from each element is employed to identify the most satisfying fitness. As shown in Figure 9, a typical GEP procedure involves several successive steps. The first step is initialization as the generation of the initial population takes place by a group of random chromosomes. The next step is the fitness evaluation concerning the fitness quantities of all chromosomes, which are problem-dependent values affecting the model performance. After the evaluation of fitness, selection and replication are carried out, where different approaches can be employed for selecting better chromosomes to create the next generation population.[148] The process of

https://doi.org/10.1021/acsomega.4c06610
ACS Omega 2025, 10, 6470−6501

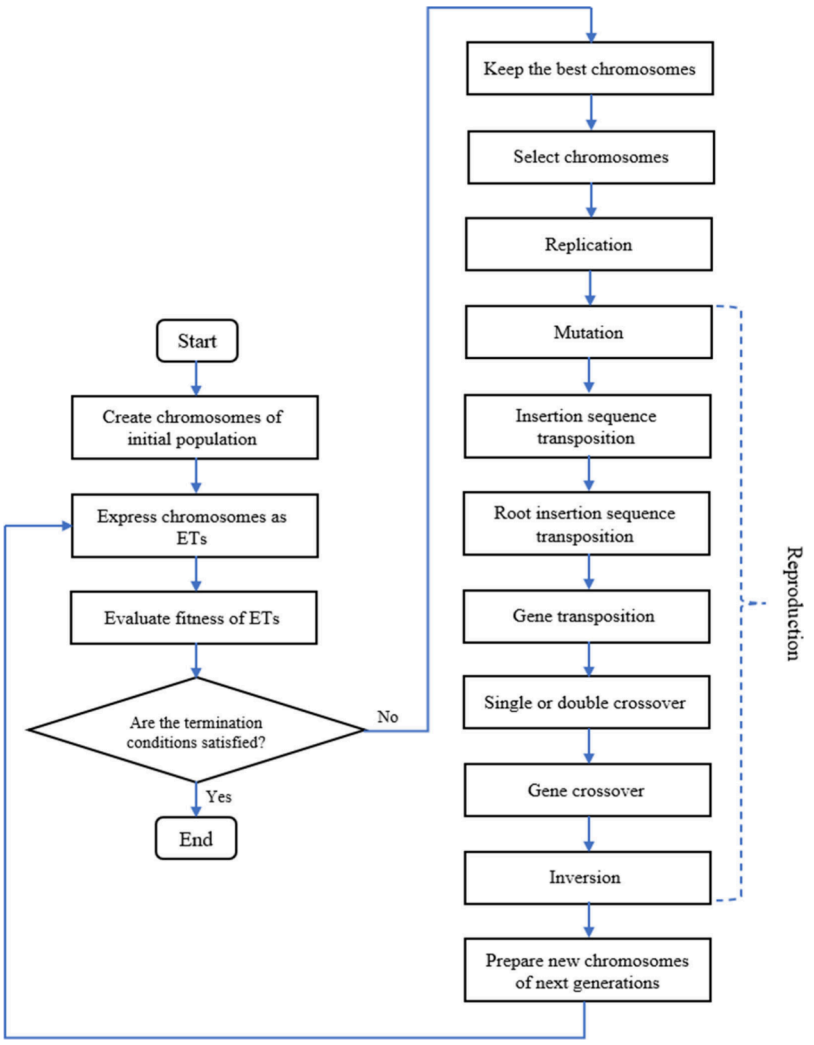

Figure 9. Algorithm of a GEP model.[107] Adapted from ref 107.

reproduction always results in valid structure, leading to a well-organized solution for utilized genetic operators.[149]

4. METHODOLOGY

This study analyzes the torrefaction process of lignocellulosic biomass using three ML hybrid methods: ANN-PSO, ANFIS, and CSA-LSSVM. In addition, a mathematical equation is developed using GEP to relate different operating variables. It performed parametric sensitivity analysis to determine the degree of impact (significance) of each input variable on the targeted output.

4.1. Data Treatment. The number and quality of data play critical roles in the successful development of ML models. More than 800 data points are used for the development of the models in this study. The data was collected from the research works on the torrefaction process of lignocellulosic biomass (e.g., agricultural and forestry residues and energy crops) carried out by Onsree et al.[55] The input data/parameters are categorized into biomass properties and torrefaction operating conditions. The input variables are time (t), temperature (T), volume fraction (in reacting gas) of CO_2, O_2, and N_2, moisture content (MC), volatile matter (VM), fixed carbon (FC), ash, content of C, H, N, and O, and sample size, and the output variable is solid yield (SY). Time and temperature have varying impacts on the torrefaction process.[150−153] For example, the effect of temperature on the torrefaction process of spruce wood is higher than that of time.[154] The concentrations of CO_2,[155−157] O_2,[55,158,159] and N_2[160,161] in the reacting gas influence the torrefaction process. In the torrefaction of forest residues, N_2 yielded a higher solid mass compared to CO_2.[162] Oxidative torrefaction of wheat straw led to higher heating value (HHV) of type C sub-bituminous carbon with minimum loss in the mass and energy yields and minimum requirement for reaction temperature and retention time, resulting in the reduction of operating costs.[163] Oxidative torrefaction of microalgae could result in an energy-efficient and cost-effective process.[164] In the torrefaction pretreatment of waste biomass (Yunnan pine; *Pinus yunnanensis*), the N_2 atmosphere added to HZSM-5 catalyst considerably improved the HC compounds conversion.[165] Moisture content (MC) is another important parameter in the torrefaction process.[166,167] In the torrefaction of corn stover biomass, MC significantly influenced the mass, energy yield, and energy density, and its impact was more noticeable at lower temperatures.[168] In another study on the torrefaction of empty fruit bunches, a significant increase in the torrefied biomass yield occurred at the feedstock's reduced MC.[169] Temperature and MC can significantly impact the CO_2 emission in a torrefaction process.[45] VM is one of the crucial parameters in the analysis of a torrefaction process.[44,170] VM removal connected to thermochemical processes can enrich

https://doi.org/10.1021/acsomega.4c06610
ACS Omega 2025, 10, 6470−6501

the HHV values of volatile bituminous coal.[171] In the torrefaction of pine sawdust, the yield of soot and carbon deposit is highly related to the VM in the feedstocks.[172] It was reported that the VM significantly decreased after increasing the temperature of the torrefaction process of rice straw (non-woody biomass). Moreover, the biochars from the rape stalk were lower than biochars from the rice straw because the high content of VM produced higher amounts of gases and liquid during the torrefaction process.[173] In the analysis of a torrefaction process, FC is another central parameter.[25,174,175] Devolatilization in a torrefaction process can form additional FC and volatilize the volatiles.[176] In the torrefaction of fruit peel waste, the FC and ash increased gradually for both *Ananas comosus* peel biochar and *Annona squamosa* peel biochar when time and temperature increased.[177] The FC and ash content increased and the VM content of the torrefied kraft pulp mills sludges decreased as time and temperature increased.[178] The same results were achieved in the torrefaction of rubberwood waste.[153] In the investigation of a torrefaction process, ash is another important parameter.[179,180] Biomass torrefaction and co-combustion can potentially decrease the tendency of ash fouling through biomass combustion, given that they decrease the deposits of the inside fouling, which can pose operational problems.[17] The results of a study (solvent extraction and torrefaction as biomass pretreatments) show that solvent extraction was influential in producing ash-less biomass.[181] In another study, torrefaction pretreatment reduced ash deposition and particular matter emissions during biomass combustion.[182] Analyzing product properties in a torrefaction process as a biomass pretreatment is a key approach to determining its mechanism.[183,184] Experiments at various operating conditions need to be carried out to evaluate the process optimization, especially via the chemical analysis (i.e., C, H, N, O, and ash) throughout the torrefaction progress.[185] In the torrefaction process of Norway spruce stem wood, stump, and bark, chemical compositions of torrefied biomass significantly changed with the torrefaction severity increase. For instance, the hemicellulose content of stem wood and stump considerably reduced at a specified temperature of 300 °C and a resident time of 60 min.[186] As another example, in the torrefaction process of rice husk, the ratios of O/C, H/C, mass, and energy yield significantly decreased at a small concentration of O_2 (e.g., 2%).[187] In another study on the torrefaction of maize, the elemental composition (C, H, N, O, K, S, and Cl) of the torrefied biomass was analyzed and concluded that the alterations in the torrefaction operating conditions did not affect the contents of K, S, and Cl significantly.[151] The elemental compositions of biomass might vary during the process. For example, in the torrefaction process of rice husk, the distribution of the typical elements (i.e., oxygen, hydrogen, and carbon) showed that the values of O/C and H/C initially decreased and thereafter increased as the severity of torrefaction enhanced.[188] Currently, the main obstacle for the economical production of second-generation biofuels is the handling and transport of biomass powders/particles. From an industrial viewpoint, the most important problem in the continuous biomass valorization process is feeding to the reaction.[189] Description of biomass particle size distribution is critical while analyzing a torrefaction process (e.g., woody biomass), especially for a commercial scale torrefaction at high temperature and residence times (e.g., a larger particle size of a biomass leads to lower liquid yield and larger char production[190]).[153,191−193] For example, in the mild pyrolysis and straw torrefaction, at smaller particle size, the Cl release ratio increased.[194] In another study, in the torrefaction of oil palm residual biomass for a given temperature, the particle size influences the solid mass yield, verifying the critical impact of volatile−solid interactions.[46] A study revealed that increasing the particle size and the torrefaction degree increased the consumption of energy for forming torrefied pellets and decreasing the particle size could improve the torrefied pellets quality (hardness and hydrophobicity).[195] The solid yield or recovery is one of the key parameters in the torrefaction process analysis.[196−201] Solid yield is calculated using the mass of material before and after the torrefaction process.[202]

4.2. Modeling Tools. The hybrid models of ANN-PSO, ANFIS, and CSA-LSSVM were developed using MATLAB software. To obtain the best results, the key parameters of each model are optimized, and the optimal values are employed to give the most suitable outcomes. GeneXproTool5 5.0 software is utilized to develop the GEP model, and the best results are achieved by running the software at different values of the critical parameters of the model. In all models, the input parameters and the output parameters are scrutinized for all described models. However, a critical concern was dealing with data on dramatically different scales. The purpose of the normalization is that each data point has the same scale, making each feature equally important.[203,204] Therefore, the data of this study is normalized within $[-1, 1]$ to avoid the numerical overflow in the runs of each program/code and to facilitate/ease the convergence process. Moreover, it eliminates the adverse impacts of adopting various units of inputs.[205] The data normalization is carried out using eq 27, as given below:

$$\hat{x} = 2\frac{x_i - x_{\min}}{x_{\max} - x_{\min}} - 1 \tag{27}$$

where $\hat{x}$ denotes the normalized value of x_i, and $x_{\max}$ and $x_{\min}$ refer to the maximum and minimum values of the data, respectively.

4.3. Assessment of Models Performance. The results of each model need to be evaluated to determine its accuracy and effectiveness. Moreover, these metrics can help to compare the different models/algorithms. It can be determined by statistical metrics such as average absolute relative error percentage (AARE%), mean square error (MSE), and coefficient of determination (R^2). The equations representing the mentioned metrics are:[206−209]

$$R^2 = 1 - \frac{\sum_{i=1}^{N}(x_d^i - x_m^i)^2}{\sum_{i=1}^{nN}(x_d^i - \overline{x})^2} \tag{28}$$

$$\mathrm{MSE} = \frac{1}{N}\sum_{i=1}^{N}(x_d^i - x_m^i)^2 \tag{29}$$

$$\mathrm{AARE\%} = 100\sum_{i=1}^{N}\left|\frac{x_d^i - x_m^i}{x_d^i}\right|/N \tag{30}$$

where x_d^i and x_m^i are the values of the data and the predicted values, $\overline{x}$ symbolizes the average value of the data, and N refers to the number of data points.

5. RESULTS AND DISCUSSION

The performance of each model is discussed separately, and the results are presented in tables and figures. The models'

https://doi.org/10.1021/acsomega.4c06610
ACS Omega 2025, 10, 6470−6501

capability in the training and testing phases is evaluated, and the results are justified based on the torrefaction process features and the characteristics of the applied model. The models are compared, and the best model is identified based on the statistical metrics. Finally, the parametric sensitivity analysis is implemented using the most accurate and suitable model to determine the degrees of impact of different operating and input parameters on the target/output parameter.

5.1. ANN-PSO. The parameters of the PSO algorithm significantly affect the configuration/performance of the ANN-PSO model. Different values of PSO parameters are used to tune the parameters (e.g., p_{best}, g_{best}, and the number of particles). The algorithm assesses the MSE value at each run, and the best values for achieving the lowest MSE are 275 for the number of particles, 1.4 for the cognition coefficient, and 2.6 for the social coefficient. Figure 10 depicts the ANN-PSO

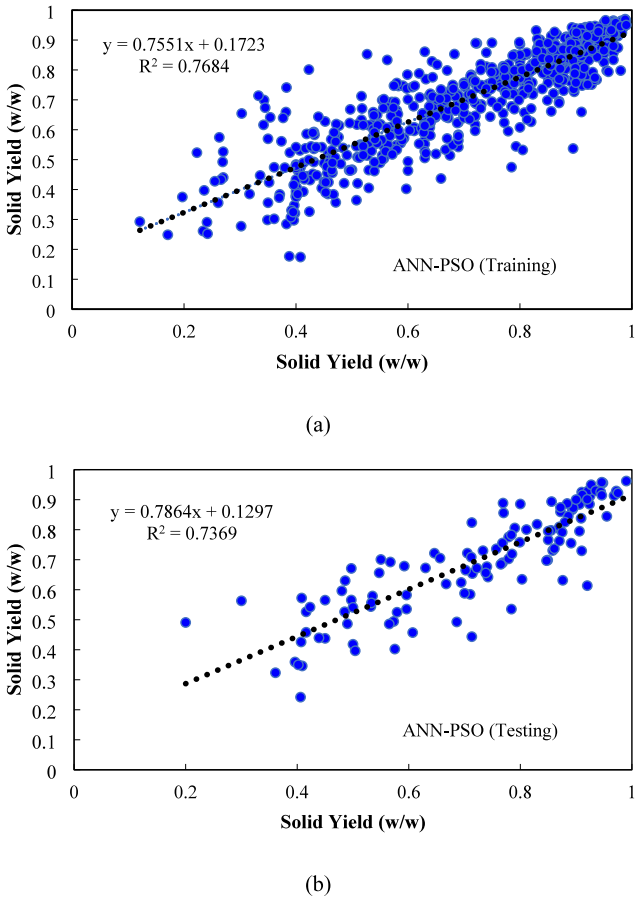

Figure 10. Performance of the ANN-PSO model: (a) training phase; (b) testing phase.

model performance for the training and testing data sets. The R^2 values of the model for the training and testing phases are 0.768 and 0.737, respectively. The results indicate that the ANN-PSO performance is not accurate. The PSO has local minima, might be a suitable technique for readily differentiable functions, and might not be proper for highly complex functions/problems. In addition, its iterative convergence rate is moderate, and it is often trapped in high-dimensional spaces.[210]

5.2. ANFIS. The proper architecture of the ANFIS model is the essential and critical feature of the modeling as improper architecture might result in overfitting, underfitting, and computational overload.[87]

The ANFIS model is developed based on the Takagi–Sugeno FIS. As the fuzzy part of the model uses If–Then rules and linguistic terms, it can learn from the data. Table 3 contains the details of the developed ANFIS model. The type of MF employed for ANFIS model development is Gaussian. MF signifies the degree or range of an independent parameter that forms part of a set. Figure 11 illustrates the MFs of the input parameters after the training process is performed. Gaussian MFs are used as they produce the minimum error throughout calibration.[211] Gaussian MFs offer steady transition between levels to open a change to fire the rules maximum number in the rule base; therefore, the representation of the relationship between inputs and output is more accurate.[212] Figure 12 shows the performance of the developed model. The R^2 values of the ANFIS model for the training and testing phases are 0.9852 and 0.8478, respectively, indicating that the ANFIS model can satisfactorily establish the input–output relationships. ANFIS is usually employed in nonlinear data applications.[213] It is an efficient technique for nonlinear processes.[214] ANFIS can perform accurate inference in complex systems. Moreover, it is flexible and offers efficient solutions for addressing uncertainty.[215]

Table 3. Features of the Developed ANFIS Model

Parameter	Definition/Value
Number of inputs	14
Number of outputs	1
Fuzzy type	Sugeno
FIS generation	Grid partition
Optimization method	Hybrid
Membership function	Gaussian
Number of fuzzy rules	12
Maximum number of epochs	2000
Initial step size	0.05
Increase rate of step size	1.1
Decrease rate of step size	0.9

5.3. CSA-LSSVM. The values of the regularization parameter (γ) and the kernel function width (tuning parameter) (σ^2) significantly impact the accuracy of LSSVM performance.[216] The optimal values of these two parameters are identified by the CSA optimization algorithm. The optimal values of γ and σ^2 are 1678.92 and 1.523, respectively. Figure 13 shows the performance of the CSA-LSSVM model for the training and testing data sets. The R^2 values of the model for the training and testing steps are 0.9839 and 0.9200, respectively. This model has significant performance. LSSVM is a modified form of SVM, which significantly simplifies the problem such that the solution is defined/characterized by a linear system.[217] The CSA framework linked with LSSVM provides an automatic search for the LSSVM optimal parameters once the training phase starts. CSA is fast and can find the global minima by running away from the local minima.[91]

5.4. GEP. There are several parameters that affect the accuracy of the GEP model. Numerous runs are carried out to obtain the most suitable model utilizing the process data and the best fitness. The model accuracy improves with an increase in the number of chromosomes and genes. There is no

https://doi.org/10.1021/acsomega.4c06610
ACS Omega 2025, 10, 6470−6501

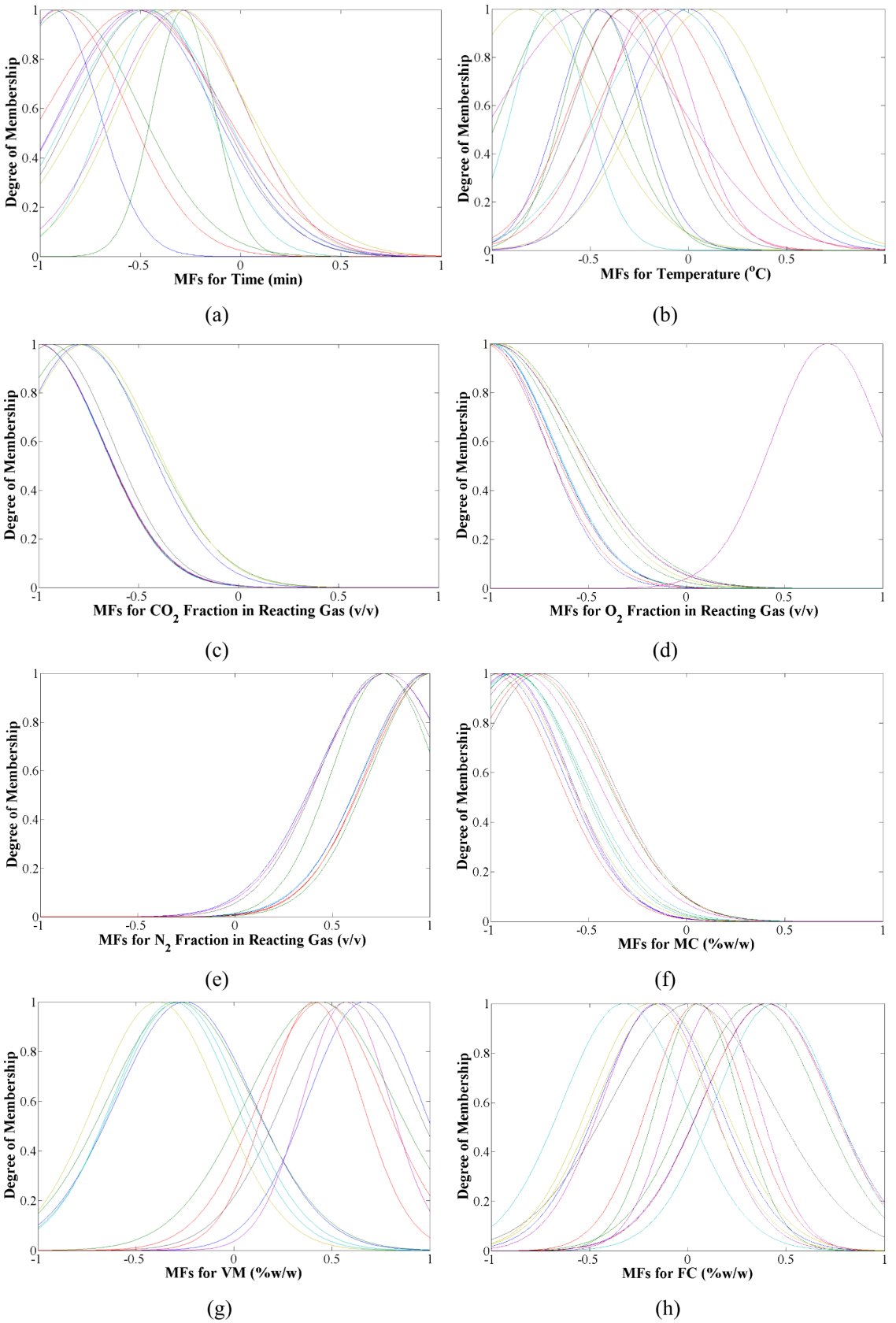

Figure 11. continued

https://doi.org/10.1021/acsomega.4c06610
ACS Omega 2025, 10, 6470−6501

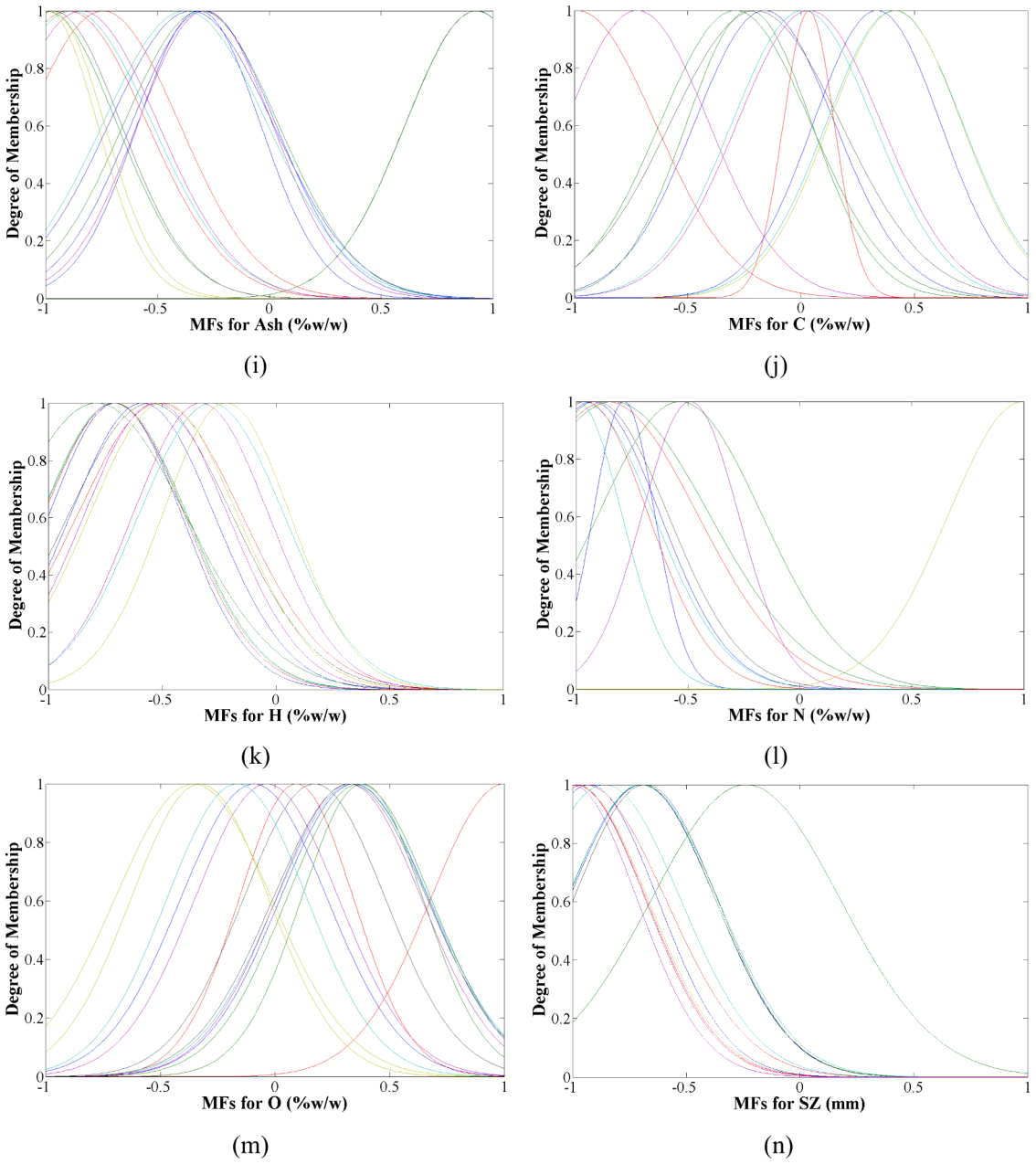

Figure 11. Membership Functions (MFs) for the input parameters of the ANFIS model: (a) time; (b) temperature; (c) CO_2 fraction in reacting gas; (d) O_2 fraction in reacting gas; (e) N_2 fraction in reacting gas; (f) moisture content (MC); (g) volatile matter (VM); (h) fixed carbon (FC); (i) ash; (j) carbon content (C); (k) hydrogen content (H); (l) nitrogen content (N); (m) oxygen content (O); (n) sample size (SZ).

significant change in the model performance by a perturbation in the head size.

Table 4 contains the values of critical parameters obtained for determining the most optimal GEP model. Figure 14 shows the performance of the GEP model using GeneXproTool5 version 5.0 software. The R^2 values of the model for the training and testing steps are 0.9149 and 0.9247, respectively.

Figure 15 exhibits the ETs of the developed GEP model according to the specifications, which are condensed in Table 4.

Numerous runs are completed in the software to determine the most suitable correlation that can accurately reflect the torrefaction process of the lignocellulosic biomass. The resulting correlation is formulated below:

$$\begin{aligned} SY = {} & \frac{\sqrt[3]{(\tanh(t) - \min(T, CC))^4} + \max\left(T, \frac{1}{\frac{MC + G1}{2.0}}\right)}{2} \\ & + \sqrt[3]{\sqrt[3]{1 - (1 - \max(CN^2 \times G2, FC \times CO))^2}} \\ & + \min(\min(T, MC), \min((\max((CO - t), CN) \\ & - (FC \times T)), CH)) \\ & + \frac{1}{\left(-\frac{\operatorname{atan}(\max(CO2 + t + G3, MC - G4))}{2}\right)^{-1}} \end{aligned} \quad (31)$$

where t stands for the time in min, T denotes the temperature in °C, CC refers to the carbon content in % w/w, MC defines the moisture content in % w/w, CN represents the nitrogen

https://doi.org/10.1021/acsomega.4c06610
ACS Omega 2025, 10, 6470−6501

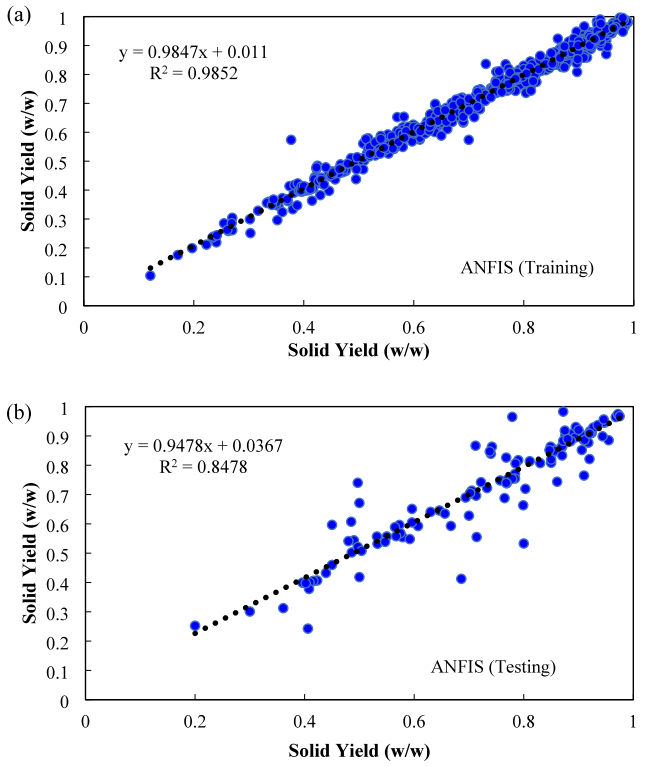

Figure 12. Performance of the ANFIS model: (a) training phase; (b) testing phase.

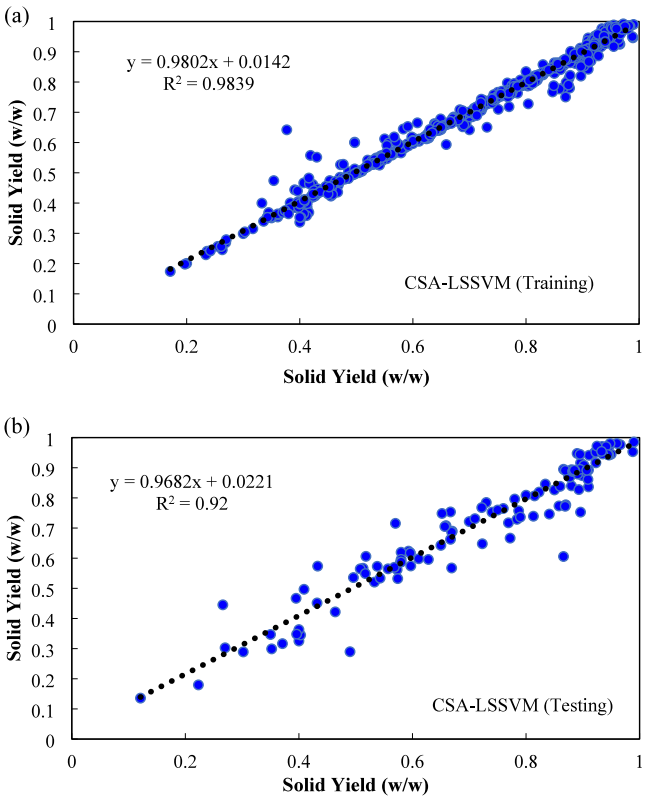

Figure 13. Performance of the CSA-LSSVM model: (a) training phase; (b) testing phase.

content in % *w*/*w*, FC symbolizes the fixed carbon in % *w*/*w*, CO represents the oxygen content in % *w*/*w*, CH is the

Table 4. GEP Model Specifications

Parameter	Value
Chromosome	95
Gene	12
Head size	7
Root insertion sequence transposition	0.00546
Mutation rate	0.00138
Gene transposition	0.00277
Inversion rate	0.00546
Insertion sequence transposition	0.00546
Random chromosome	0.0026
Fixed-root mutation	0.00068
Constant fine-tuning	0.00206

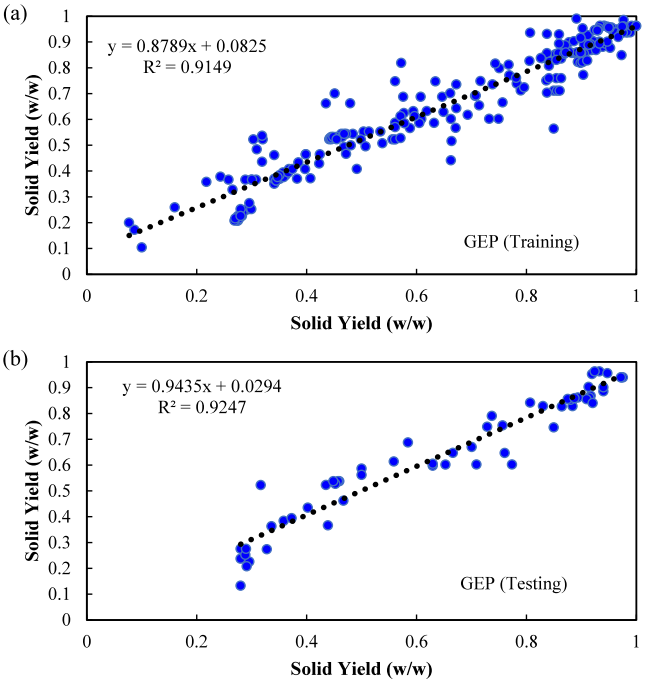

Figure 14. GEP model performance: (a) training phase; (b) testing phase.

hydrogen content in % *w*/*w*, CO2 reveals the oxygen fraction in the reacting gas in *v*/*v*, and SY introduces the solid yield in *w*/*w*. *G*1, *G*2, *G*3, and *G*4 are constant values of 3.7717, 1.9854, −0.0578, and −0.1087, respectively.

Considering the highest accuracy of the runs completed in GeneXproTool5 5.0 software, the most important operating parameters are determined and depicted in Figure 16.

5.5. Comparison of Models. Different statistical metrics, including coefficient of determination (R^2), mean square error (MSE), and average absolute relative error percent (AARE%), are used to assess the performance of the developed models. Table 5 contains the performance of the developed models according to the utilized statistical metrics, revealing that the CSA-LSSVM is the most accurate predictive tool. The R^2, MSE, and AARE% values of the CSA-LSSVM performance are 0.98, 0.00082, and 2.61, respectively. Figure 17 displays the performance of ANN-PSO, ANFIS, and CSA-LSSVM, illustrating the target value and the predicted value for the training and testing steps. Figure 17 also shows the performance of the GEP models, portraying the target value and the resulting value from the presented model. It can be

https://doi.org/10.1021/acsomega.4c06610
ACS Omega 2025, 10, 6470−6501

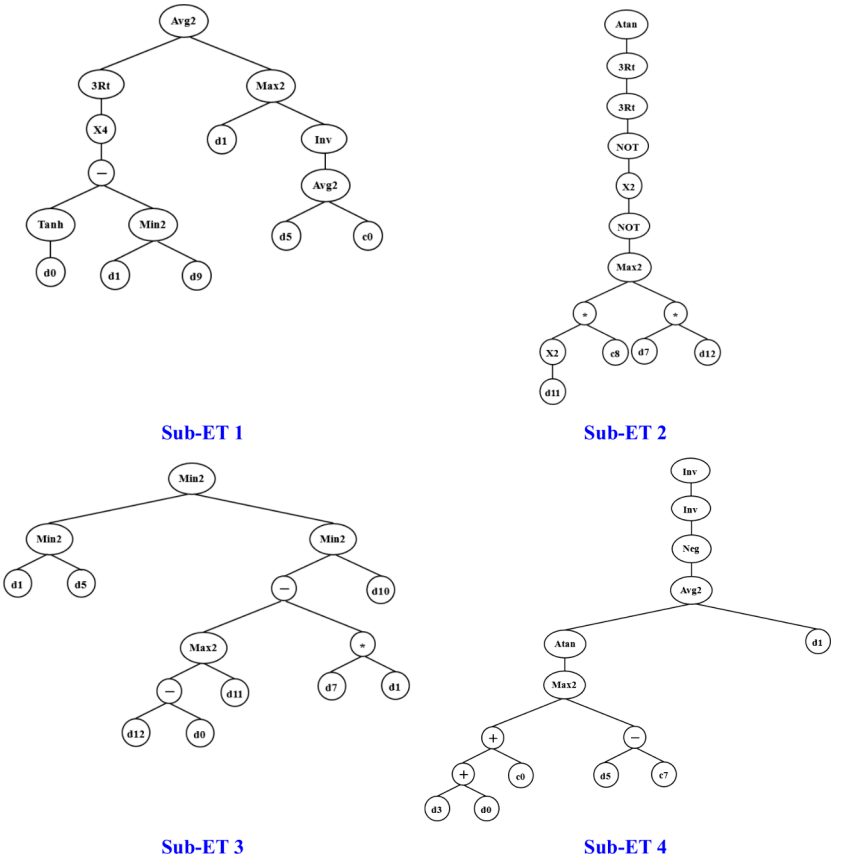

Figure 15. Expression tree of the developed gene expression programming (GEP) model: variables (d) and constant parameters (c).

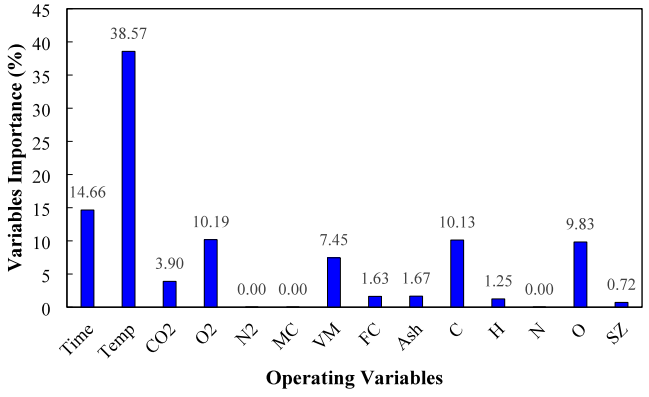

Figure 16. Degrees of importance of the involved operating variables influencing the targeted parameter.

observed that there is a better fit between the predicted values and the experimental data for the solid yield obtained from CSA-LSSVM compared to ANN-PSO, ANFIS, and GEP models.

The best result with a R^2 value of about 0.90 is obtained while utilizing Gradient tree boosting algorithm.[55] Therefore, this research is more accurate than the study reported in the literature, revealing the superiority of the introduced models, particularly CSA-LSSVM. In a similar study on the prediction of biochar properties from LB torrefaction (biochar derived from lignocellulosic biomass torrefaction), the best result was achieved by Gradient boosting machines with a R^2 value of 0.94, which is less accurate than the current research.[20]

5.6. Sensitivity Analysis of Results. The degrees of impact of different parameters on the torrefaction process, mainly the solid yield as the targeted output, are implemented using the most accurate model, which is CSA-LSSVM. Parametric sensitivity analysis (PSA) is carried out to find out the interrelation of the input and output parameters.[218−220] In the setting of probability and statistics, the degree of linear relationship between two variables is determined by correlation matrix theory in a multivariable system.[221] A correlation analysis is usually determined by relating to a correlation coefficient. It relates the direction and strength of a linear correlation between an uncertain variable and the output. The correlation analysis format is to verify a group of variables and to alter each variable individually while maintaining the other variables at the original amounts. The most recognized correlation coefficient is the Pearson correlation coefficient.[222]

Table 5. Accuracy of the Developed Models

Model	R^2 (Training)	R^2 (Testing)	MSE (Training)	MSE (Testing)	AARE% (Training)	AARE% (Testing)
ANN-PSO	0.768	0.737	0.0090	0.0098	12.0776	12.4089
ANFIS	0.9852	0.8478	0.0006	0.0057	2.5532	6.7782
CSA-LSSVM	0.9839	0.9200	0.0006	0.0035	1.9575	6.8840
GEP	0.9149	0.9247	0.0056	0.0045	11.8636	10.3662

https://doi.org/10.1021/acsomega.4c06610
ACS Omega 2025, 10, 6470−6501

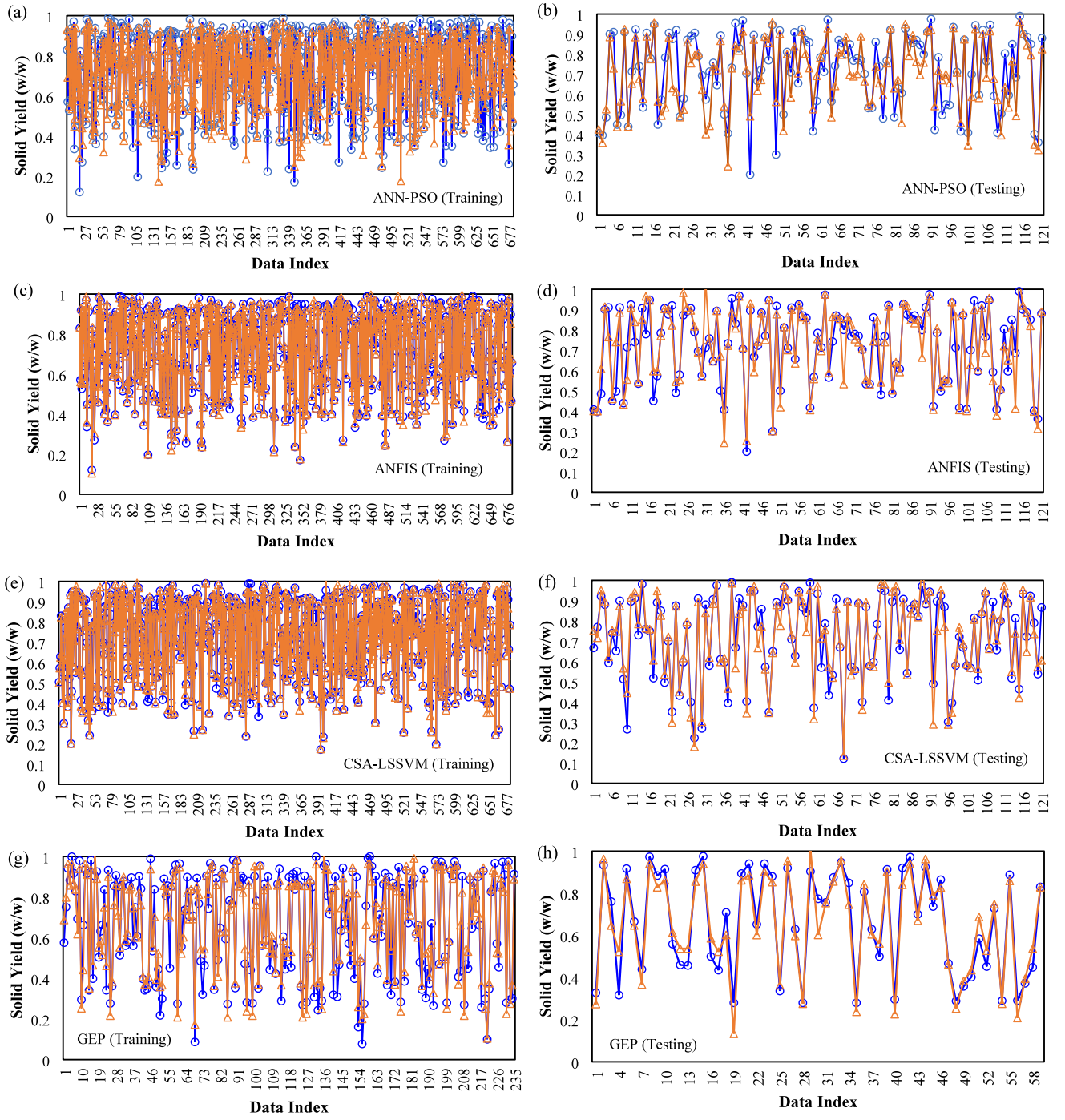

Figure 17. Comparison of the developed models: (a) ANN-PSO: training; (b) ANN-PSO: testing; (c) ANFIS: training; (d) ANFIS: testing; (e) CSA-LSSVM: training; (f) CSA-LSSVM: testing; (g) GEP: training; (h) GEP: testing (blue circles: target; orange triangles: predicted).

It is calculated by dividing the covariance of the two uncertainty criteria by the product of their standard deviations as follows:[223−225]

$$r_{x_1x_2} = \frac{\beta_{x_1x_2}}{\beta_{x_1}\beta_{x_2}} \tag{32}$$

$$\beta_x = \sqrt{\frac{\sum_{i=1}^{N}(x - \overline{x})^2}{N-1}} \tag{33}$$

$$\beta_{x_1x_2} = \frac{\sum_{i=1}^{N}(x_1 - \overline{x}_1)(x_2 - \overline{x}_2)}{N-1} \tag{34}$$

where $r_{x_1x_2}$ introduces the correlation coefficient, $\beta_{x_1x_2}$ is the covariance, β_{x_1} and β_{x_2} represent the two variables standard deviation, x_1 and x_2 are the two variables, $\overline{x}_1$ and $\overline{x}_2$ are the average values of the two variables, and n symbolizes the number of the experimental data. The calculated value for r fits into $[-1, 1]$, implying the linear relationship strength between the two variables. When the r value is near 1, it indicates a positive relationship. If the r value is near -1, it divulges a

https://doi.org/10.1021/acsomega.4c06610
ACS Omega 2025, 10, 6470−6501

negative relationship between the two variables.[226] Values close to zero indicate a weak connection between the two suggested variables. Figure 18 pictures the outcomes of the

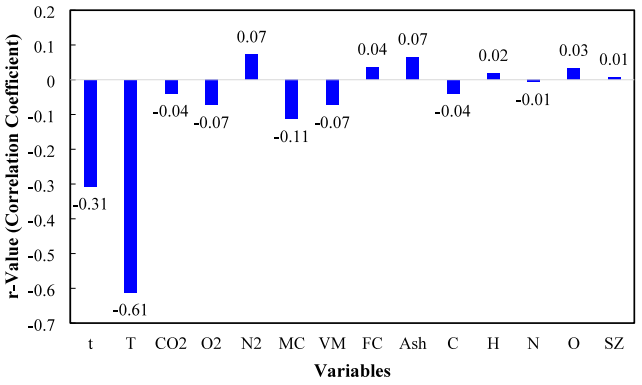

Figure 18. Correlation coefficient values indicate the linear individual relationship between the input variable indicated and the output variable.

PSA of the torrefaction process variables and the magnitude of the relationship between the input variables and the output variable (solid yield). According to Figure 18, there is a strong inverse linear relationship between the solid yield and temperature ($r = -0.61$). It means that an increase in temperature decreases the solid yield. Further, there is a negative relationship between residence time and the solid yield, revealing lower solid yield at larger residence time of operation. The influence of the SZ on the torrefaction process intensifies at higher temperatures,[8,195] as evidenced by the findings in Figure 18. Moreover, the SZ's effect becomes more pronounced with shorter torrefaction residence times. This suggests that temperature and residence time significantly control the SZ's role in torrefaction performance.[12] Typically, woody biomass contains approximately 0.68% nitrogen. In this study, the nitrogen content of the LB ranges from 0 to 3.9% *w*/*w*. As a result, changes in nitrogen forms (e.g., pyridinic-N, pyrrolic-N, and quaternary-N) during torrefaction are likely minimal, especially at lower temperatures.[8,12] These findings conform to those obtained from the GEP model, as illustrated in Figure 16.

The analysis of torrefied biomass as an enriched solid fuel is essential before any application. In the field of wood and fuel sciences, various methods have been utilized to characterize and evaluate solid fuels (e.g., torrefied biomass).[227] According to this study, different operating variables are influential in the torrefaction process. Employing the hybrid ML methods and the GEP, the degrees of individual impacts of these variables have been assessed. Temperature plays the most critical role in the torrefaction process.[228,229] Residence time significantly impacts the torrefaction process. Temperature and residence time substantially impact the torrefaction process, with temperature having a more crucial impact.[230] Figure 19 shows the comparison between the SY values resulting from the GEP model and the experimental data for the two most crucial parameters of temperature and time affecting the biomass torrefaction process of LB. As the temperature increases, the solid yield decreases, and the gas and liquid product yield increases. A short residence time (i.e., 15−60 min) is sufficient for an efficient torrefaction process of biomass, and longer residence time does not impact the transformation of biomass substantially.[231] Moisture content

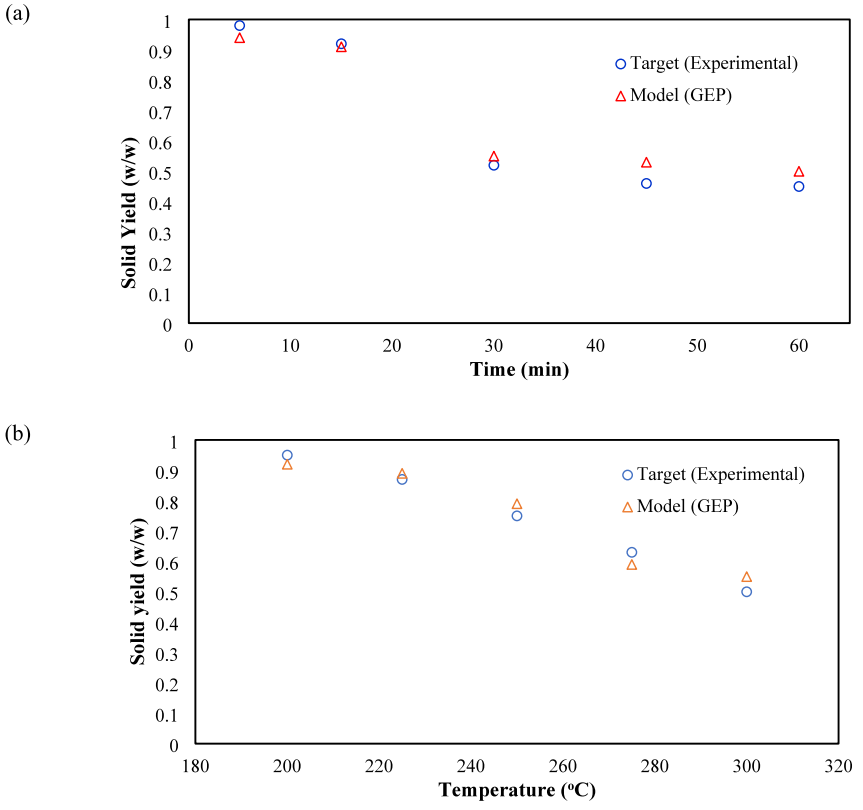

Figure 19. Comparison of the GEP model predicted values with the experimental data for the process parameters: (a) temperature; (b) time.

https://doi.org/10.1021/acsomega.4c06610
ACS Omega 2025, 10, 6470−6501

(MC) is another key factor in the torrefaction process. More stable quality and cleaner gas production can result from a lower MC of the biomass.[232] From the reaction kinetics point of view, vaporization of internal MC of the biomass is the key reaction at low temperatures.[233] Considering the results of this study, sample size is not a significant factor, especially compared to temperature and residence time. Nonetheless, in favor of heat and mass transfer throughout the torrefaction process for more efficient energy and solid yields, the particle size should be taken into consideration.[195] Based on the results, ash is at the same level of impact as VM. It seems that ash is not a critical factor; however, a biomass with a considerable amount of ash might be problematic in some operations such as boilers creating slagging, fouling, and corrosion.[234]

The solid fraction of the torrefied biomass, which is considered as the key product from the process, contains the intermediate specifications between the raw biomass and the charcoal produced from the process of carbonization performed at high temperatures.[235] Improved properties of the torrefied biomass (e.g., high heat value, CO_2 neutrality, hydrophobicity, and high energy density) advance the fast development of biomass-fired plants; however, the torrefied biomass combustion remains challenging for a number of reasons such as ash-related problems (e.g., silicate-melt-induced slagging, alkali-induced slagging, and corrosion in biomass furnaces) and economy viability.[236] Environmental feasibility analysis of the torrefaction process implies that the torrefied pellets produce substantially lower emissions in comparison with wood pellets at specific energy production.[237] Evaluation of the torrefaction byproducts via the biorefinery on a circular economy can promote the economic viability and environmental performance of the torrefied biomass. Utilization of the torrefaction process in pulverized coal-fired power plants may result in the formation of persistent organic pollutants including polychlorinated dibenzofurans and dibenzo-*p*-dioxins throughout torrefaction within the temperature range of 200−350 °C.[65]

It should be noted that the GEP model developed in this study incorporates 9 out of 14 process parameters that were used in the ANN-PSO, ANFIS, and CSA-LSSVM models. Notably, it includes the residence time and temperature, which are recognized as the most influential parameters in the torrefaction process. While the GEP-derived equation does not explicitly include the type of reactor, it captures the essential variables that govern the torrefaction process across various reactor configurations. The model's potential applicability to different types of lignocellulosic biomass stems from the fact that similar torrefaction systems are affected by similar process parameters. However, it is important to note that the current model's performance for significantly different reactor types or biomass compositions would need to be validated with additional data. Regarding particle size, we acknowledge limitations in the current data set distribution. For instance, out of 805 data points, 223 are for 18 mm particle size, 78 for 1 mm, and 108 for approximately 0.4 mm. This uneven distribution may limit the model's ability to fully capture the impact of particle size on solid yield. Future work should focus on incorporating a more balanced distribution of particle sizes to enhance the model's predictive capabilities across a wider range of conditions.

It is important to acknowledge that the AI/ML models developed in this study, while capable of predicting complex process systems, are inherently dependent on the specific experimental conditions used, including reactor type, biomass type, particle size, temperature, and residence time. However, these models offer significant advantages in capturing complex, nonlinear relationships between variables without requiring explicit modeling of all underlying phenomena. The GEP model, in particular, identifies and incorporates the most critical parameters affecting system performance, allowing for a satisfactory prediction of torrefaction process outcomes without including all possible variables. While the direct applicability of these models may be limited to the conditions under which they were developed, the methodology demonstrated in this study can serve as a template for researchers working with different types of biomass or reactor configurations. Furthermore, these models can be easily retrained or fine-tuned with additional data, potentially extending their applicability to a broader range of conditions.

6. CONCLUSIONS

Biomass feedstocks can be used to produce many chemicals and fuels. Generating power utilizing raw biomass is challenged by a low energy density, low heating value, high moisture content, high oxygen content, and low bulk density. Therefore, improving the properties of raw biomass as a substitute for fossil fuels is vital. Torrefaction as a thermochemical process can address the mentioned drawbacks through converting the raw biomass to a high-quality solid fuel. In this study, the torrefaction process of lignocellulosic biomass is evaluated using hybrid ML techniques including ANN-PSO, CSA-LSSVM, and ANFIS as well as the mathematical analysis of the process utilizing the GEP approach. The developed CSA-LSSVM method is the most accurate model with a 0.98 coefficient of determination. The ML models and the resulting correlation emphasize that temperature and residence time are the most effective variables on solid yield, with the temperature having a greater impact. The mathematical equation derived from GEP interrelates the various variables affecting the process of torrefaction of LB having coefficient of determination values of 0.9149 and 0.9247 for the training and testing phase, respectively. The developed models do not require an intricate knowledge of the kinetics of LB torrefaction and can be readily used for analyzing such processes. The findings of this study can aid in designing bioenergy production and maximizing biomass potential. These models provide a suitable platform for advancing the bioenergy industry by reducing operating costs, energy consumption, and carbon footprints. However, significant gaps remain in understanding the torrefaction process of LB. Key areas needing further research include characterizing torrefaction chemical reaction pathways, optimizing and designing suitable equipment for the process, and conducting detailed analyses of supply chain influences.

AUTHOR INFORMATION

Corresponding Author

Sohrab Zendehboudi − *Department of Process Engineering, Memorial University, St. John's, NL A1B 3X5, Canada;* orcid.org/0000-0001-8527-9087; Email: szendehboudi@mun.ca

Authors

Abbas Azarpour − *Department of Engineering and Physics, Southern Arkansas University, Magnolia, Arkansas 71753, United States;* orcid.org/0000-0001-5371-1250

https://doi.org/10.1021/acsomega.4c06610
ACS Omega 2025, 10, 6470−6501

Noori M. Cata Saady − *Department of Civil Engineering, Memorial University, St. John's, NL A1B 3X5, Canada*

Complete contact information is available at: https://pubs.acs.org/10.1021/acsomega.4c06610

Notes

The authors declare no competing financial interest.

■ ACKNOWLEDGMENTS

We acknowledge the support of Southern Arkansas University (Faculty Research Grant). Also, the financial assistance of MITACS, Memorial University, and the Natural Sciences and Engineering Research Council of Canada (NSERC) is greatly appreciated.

■ NOMENCLATURE

Abbreviations

AARE	average absolute relative error
AdB	AdaBoost
AI	artificial intelligence
ANFIS	adaptive neuro-fuzzy inference system
ANN	artificial neural network
BP	back-propagation
BPNN	back-propagation neural network
Ce	cellulose content
CF	cost function
CSA	coupled simulated annealing
DT	decision tree
ERT	extremely randomized trees
ET	expression tree
EY	energy yield
FPM	first principle model
FR	fuel ratio
FRT	forests of randomized trees
g_{best}	global best
GA	genetic algorithm
GEP	gene expression programming
GHG	greenhouse gas
GP	genetic programming
GTB	gradient tree boosting
FIS	fuzzy inference system
FL	fuzzy logic
HHV	higher heating value
Hm	hemicellulose content
IP	input parameter
k-NN	k-nearest neighbors
KRR	kernel ridge regression
LB	lignocellulosic biomass
Lg	lignin content
Lss	lasso
LSSVM	least-squares support vector machine
MAPE	mean absolute percentage error
MARS	multivariable adaptive regression splines
MF	membership function
ML	machine learning
MLP	multilayer perceptron
NRR	normal ridge regression
OP	output parameter
p_{best}	personal best
PSA	parametric sensitivity analysis
PSO	particle swarm optimization
R^2	coefficient of determination
RBF	radial basis function
RE	renewable energy
RF	random forest
SA	simulated annealing
SDR	sorghum distillery residue
SI	swarm intelligence
SM	solid mass
SVM	support vector machine
TGA	thermogravimetric analysis
TSI	torrefaction severity index
WT	wet torrefaction

Symbols

A and B	fuzzy sets
Ash	ash content in biomass (% w/w)
b	bias
C_i	concentration of component i
c_1	cognitive parameter
c_2	social parameter
CC	carbon content in biomass (% w/w)
CH	hydrogen content in biomass (% w/w)
CN	nitrogen content in biomass (% w/w)
CO	oxygen content (% w/w)
CO2	oxygen fraction in reacting gas (v/v)
CO_2	CO_2 fraction in the reacting gas (v/v)
e	regression error
FC	fixed carbon in biomass (% w/w)
G	constant value (GEP model)
hl	Head's length
K	kernel function
L	Lagrange function
k	index of iteration
MC	moisture content in biomass (% w/w)
MSE	mean square error
N	number of training data
nf	number of function's arguments
N_2	N_2 fraction in the reacting gas (v/v)
p_{gd}	best global position of particle i in dimension d
p_{id}	best personal position of particle i in dimension d
r	correlation coefficient
SY	solid yield (w/w)
SZ	sample size (biomass) (mm)
T	temperature (°C)
t	residence time (min)
tl	tail's length
VM	volatile matter in biomass (% w/w)
v_i	speed of particle i in dimension d
w	weight factor
x_{id}	position of particle i in dimension d
x	data value
x_d	data value
x_m	measured/calculated value
x_{max}	maximum value of data
x_{min}	minimum value of data
$\hat{x}$	normalized value
$\overline{x}$	average value

Greek Letters

α	Lagrange multiplier
β	covariance
γ	regularization constant
μ	membership function
σ	tuning parameter (kernel function width)
Φ	nonlinear mapping function

https://doi.org/10.1021/acsomega.4c06610
ACS Omega 2025, 10, 6470−6501

Ω kernel matrix

REFERENCES

(1) Richa, L.; Colin, B.; Pétrissans, A.; Wallace, C.; Hulette, A.; Quirino, R. L.; Chen, W.-H.; Pétrissans, M. Catalytic and char-promoting effects of potassium on lignocellulosic biomass torrefaction and pyrolysis. *Environ. Technol. Inno.* **2023**, *31*, 103193.

(2) Azarpour, A.; Mohammadzadeh, O.; Rezaei, N.; Zendehboudi, S. Current status and future prospects of renewable and sustainable energy in North America: Progress and challenges. *Energy Convers. Manage.* **2022**, *269*, 115945.

(3) Potnuri, R.; Suriapparao, D. V.; Rao, C. S.; Sridevi, V.; Kumar, A. Effect of dry torrefaction pretreatment of the microwave-assisted catalytic pyrolysis of biomass using the machine learning approach. *Renew. Energy* **2022**, *197*, 798−809.

(4) Yang, Y.; Qu, X.; Huang, G.; Ren, S.; Dong, L.; Sun, T.; Liu, P.; Li, Y.; Lei, T.; Cai, J. Insight into lignocellulosic biomass torrefaction kinetics with case study of pinewood sawdust torrefaction. *Renew. Energy* **2023**, *215*, 118941.

(5) Yang, X.; Zhao, Y.; Zhang, L.; Wang, Z.; Zhao, Z.; Zhu, W.; Ma, J.; Shen, B. Effects of torrefaction pretreatment on the structural features and combustion characteristics of biomass-based fuel. *Molecules* **2023**, *28* (12), 4732.

(6) Global Monitoring Laboratory. Trend of Carbon Dioxide Concentration. National Oceanic and Atmospheric Administration, 2024. https://gml.noaa.gov/ccgg/trends/global.html (accessed May 27, 2024).

(7) Slezak, R.; Unyay, H.; Szufa, S.; Ledakowicz, S. An extensive review and comparison of modern biomass reactors torrefaction vs. biomass pyrolizers—Part 2. *Energies* **2023**, *16* (5), 2212.

(8) He, Y.; Zhang, S.; Liu, D.; Xie, X.; Li, B. Effect of biomass particle size on the torrefaction characteristics in a fixed-bed reactor. *Energies* **2023**, *16* (3), 1104.

(9) Ercan, B.; Alper, K.; Ucar, S.; Karagoz, S. Comparative studies of hydrochars and biochars produced from lignocellulosic biomass via hydrothermal carbonization, torrefaction and pyrolysis. *J. Energy Inst.* **2023**, *109*, 101298.

(10) Azarpour, A.; Zendehboudi, S.; Mohammadzadeh, O.; Rajabzadeh, A. R.; Chatzis, I. A review on microalgal biomass and biodiesel production through Co-cultivation strategy. *Energy Convers. Manage.* **2022**, *267*, 115757.

(11) Mamvura, T. A.; Danha, G. Biomass torrefaction as an emerging technology to aid in energy production. *Heliyon* **2020**, *6* (3), No. e03531.

(12) Riaz, S.; Al-Abdeli, Y. M.; Oluwoye, I. Partially oxidative torrefaction of woody biomass pellets: Burning behaviour and emission analysis. *BioEnergy Res.* **2023**, *16*, 2331−2341.

(13) Liu, G.; Zhang, R.; Zhang, B.; Liu, J.; Wu, Z.; Wang, Z.; Yang, F.; Yang, B. Performance evaluation of torrefaction coupled with a chemical looping gasification process under autothermal conditions: Flexible syngas production from biomass. *Energy Fuel.* **2023**, *37* (1), 424−438.

(14) Kim, H.; Yu, S.; Ra, H.; Yoon, S.; Ryu, C. Prediction of pyrolysis kinetics for torrefied biomass based on raw biomass properties and torrefaction severity. *Energy* **2023**, *278*, 127759.

(15) Guo, S.; Liu, L.; Zhao, D.; Zhao, C.; Li, X.; Li, G. Optimization of briquette fuels by co-torrefaction of residual biomass and plastic waste using response surface methodology. *Molecules* **2023**, *28* (6), 2568.

(16) Lin, Y.-Y.; Chen, W.-H.; Colin, B.; Petrissans, A.; Quirino, R. L.; Petrissans, M. Thermodegradation characterization of hardwoods and softwoods in torrefaction and transition zone between torrefaction and pyrolysis. *Fuel* **2022**, *310*, 122281.

(17) Han, J.; Yu, D.; Wu, J.; Yu, X.; Liu, F.; Xu, M. Effects of torrefaction on ash-related issues during biomass combustion and co-combustion with coal. Part 2: Ash fouling behavior. *Fuel* **2023**, *334*, 126777.

(18) Peduzzi, E.; Boissonnet, G.; Haarlemmer, G.; Dupont, C.; Maréchal, F. Torrefaction modelling for lignocellulosic biomass conversion processes. *Energy* **2014**, *70*, 58−67.

(19) de Oliveira Brotto, J.; Cruz, T. A.; de Oliveira Pereira, I.; Ienczak, J. L.; Peralta, R. A.; Lázaro-Martínez, J. M.; José, H. J.; Rodríguez-Castellón, E.; Moreira, R. d. F. P. M. Mechanistic insights and kinetics of torrefaction of pine wood biomasses using solid-state NMR. *J. Anal. Appl. Pyrolysis* **2023**, *172*, 106019.

(20) Su, G.; Jiang, P. Machine learning models for predicting biochar properties from lignocellulosic biomass torrefaction. *Bioresour. Technol.* **2024**, *399*, 130519.

(21) Soria-Verdugo, A.; Cano-Pleite, E.; Panahi, A.; Ghoniem, A. F. Kinetics mechanism of inert and oxidative torrefaction of biomass. *Energy Convers. Manage.* **2022**, *267*, 115892.

(22) Ivanovski, M.; Goricanec, D.; Krope, J.; Urbancl, D. Torrefaction pretreatment of lignocellulosic biomass for sustainable solid biofuel production. *Energy* **2022**, *240*, 122483.

(23) Kuzmin, S.; Isemin, R.; Mikhalev, A.; Milovanov, O. Y.; Klimov, D.; Muratova, N.; Kokh-Tatarenko, V.; Nebyvayev, A. Results of comparative studies of treatment processes of some types of biomass by wet and oxidative torrefaction methods. *Chem. Petrol. Eng.* **2022**, *58* (7−8), 581−587.

(24) Watts, J.; Potter, A.; Mohan, V.; Kumari, P.; Thengane, S. K.; Sokhansanj, S.; Cao, Y.; Kung, K. S. Proxy quality control of biomass particles using thermogravimetric analysis and Gaussian process regression models. *Biofuel. Bioprod. Biorefin.* **2023**, *17*, 1274−1289.

(25) Zheng, K.; Han, H.; Hu, S.; Ren, Q.; Su, S.; Wang, Y.; Jiang, L.; Xu, J.; Li, H.; Tong, Y. Upgrading biomass waste to bio-coking coal by pressurized torrefaction: Synergistic effect between corncob and lignin. *Energy* **2023**, *267*, 126536.

(26) Director, L.; Sinelshchikov, V. Numerical modeling of torrefaction reactor integrated in energy technological complex. *Energy* **2019**, *167*, 1194−1204.

(27) Sarvaramini, A.; Larachi, F. c. a. Pyrolysis Kinetics of Pre-Torrefied Woody Biomass Based on Torrefaction Severity-Experiments and Model Verification. *Ind. Eng. Chem. Res.* **2017**, *56* (45), 12972−12983.

(28) Regmi, B.; Arku, P.; Tasnim, S. H.; Mahmud, S.; Dutta, A. Modelling of heat transfer during torrefaction of large lignocellulosic biomass. *Heat Mass Transfer.* **2018**, *54*, 1989−1997.

(29) Brachi, P.; Chirone, R.; Miccio, F.; Miccio, M.; Ruoppolo, G. Entrained-flow gasification of torrefied tomato peels: Combining torrefaction experiments with chemical equilibrium modeling for gasification. *Fuel* **2018**, *220*, 744−753.

(30) Kung, K. S.; Ghoniem, A. F. A decentralized biomass torrefaction reactor concept. Part II: Mathematical model and scaling law. *Biomass Bioenergy* **2019**, *125*, 204−211.

(31) Oh, K. C.; Kim, J.; Park, S. Y.; Kim, S. J.; Cho, L. H.; Lee, C. G.; Roh, J.; Kim, D. H. Development and validation of torrefaction optimization model applied element content prediction of biomass. *Energy* **2021**, *214*, 119027.

(32) Luo, H.; Wang, X.; Krochmalny, K.; Niedzwiecki, L.; Czajka, K.; Pawlak-Kruczek, H.; Wu, X.; Liu, X.; Xiong, Q. Assessments and analysis of lumped and detailed pyrolysis kinetics for biomass torrefaction with particle-scale modeling. *Biomass Bioenergy* **2022**, *166*, 106619.

(33) Feng, Y.; Qiu, K.; Zhang, Z.; Li, C.; Rahman, M. M.; Cai, J. Distributed activation energy model for lignocellulosic biomass torrefaction kinetics with combined heating program. *Energy* **2022**, *239*, 122228.

(34) Yousuf, A. Biodiesel from lignocellulosic biomass-prospects and challenges. *Waste Manage. (Oxford)* **2012**, *32* (11), 2061−2067.

(35) Sawatdeenarunat, C.; Surendra, K.; Takara, D.; Oechsner, H.; Khanal, S. K. Anaerobic digestion of lignocellulosic biomass: challenges and opportunities. *Bioresour. Technol.* **2015**, *178*, 178−186.

(36) Dashti, A.; Raji, M.; Razmi, A.; Rezaei, N.; Zendehboudi, S.; Asghari, M. Efficient hybrid modeling of CO_2 absorption in aqueous solution of piperazine: Applications to energy and environment. *Chem. Eng. Res. Des.* **2019**, *144*, 405−417.

https://doi.org/10.1021/acsomega.4c06610
ACS Omega 2025, 10, 6470−6501

(37) Zare, M.; Zendehboudi, S.; Abdi, M. A. Deterministic tools to estimate induction time for methane hydrate formation in the presence of Luvicap 55 W solutions. *J. Mol. Liq.* **2022**, *348*, 118374.
(38) Bates, R. B.; Ghoniem, A. F. Biomass torrefaction: Modeling of reaction thermochemistry. *Bioresour. Technol.* **2013**, *134*, 331−340.
(39) Gogoi, M.; Konwar, K.; Bhuyan, N.; Borah, R. C.; Kalita, A. C.; Nath, H. P.; Saikia, N. Assessments of pyrolysis kinetics and mechanisms of biomass residues using thermogravimetry. *Bioresour. Technol. Rep.* **2018**, *4*, 40−49.
(40) Sarvaramini, A.; Assima, G. P.; Larachi, F. Dry torrefaction of biomass-Torrefied products and torrefaction kinetics using the distributed activation energy model. *Chem. Eng. J.* **2013**, *229*, 498−507.
(41) Rajabzadeh, A. R.; Ruzich, N.; Zendehboudi, S.; Rahbari, M. Biomass leachate treatment and nutrient recovery using reverse osmosis: experimental study and hybrid artificial neural network modeling. *Energy Fuel.* **2012**, *26* (12), 7155−7163.
(42) Bach, Q.-V.; Tran, K.-Q.; Skreiberg, Ø.; Trinh, T. T. Effects of wet torrefaction on pyrolysis of woody biomass fuels. *Energy* **2015**, *88*, 443−456.
(43) Granados, D.; Chejne, F.; Basu, P. A two dimensional model for torrefaction of large biomass particles. *J. Anal. Appl. Pyrolysis* **2016**, *120*, 1−14.
(44) Granados, D.; Basu, P.; Chejne, F. Biomass torrefaction in a two-stage rotary reactor: modeling and experimental validation. *Energy Fuel.* **2017**, *31* (5), 5701−5709.
(45) Haseli, Y. Process modeling of a biomass torrefaction plant. *Energy Fuel.* **2018**, *32* (4), 5611−5622.
(46) Talero, G.; Rincón, S.; Gómez, A. Torrefaction of oil palm residual biomass: Thermogravimetric characterization. *Fuel* **2019**, *242*, 496−506.
(47) Dacres, O. D.; Tong, S.; Li, X.; Zhu, X.; Edreis, E. M.; Liu, H.; Luo, G.; Worasuwannarak, N.; Kerdsuwan, S.; Fungtammasan, B. Pyrolysis kinetics of biomasses pretreated by gas-pressurized torrefaction. *Energy Convers. Manage.* **2019**, *182*, 117−125.
(48) Duan, H.; Zhang, Z.; Rahman, M. M.; Guo, X.; Zhang, X.; Cai, J. Insight into torrefaction of woody biomass: Kinetic modeling using pattern search method. *Energy* **2020**, *201*, 117648.
(49) Gonzalez Martinez, M.; Dupont, C.; Anca-Couce, A.; da Silva Perez, D.; Boissonnet, G.; Thiery, S.; Meyer, X.-m.; Gourdon, C. Understanding the torrefaction of woody and agricultural biomasses through their extracted macromolecular components. Part 2: Torrefaction model. *Energy* **2020**, *210*, 118451.
(50) Barontini, F.; Biagini, E.; Tognotti, L. Influence of torrefaction on biomass devolatilization. *ACS Omega* **2021**, *6* (31), 20264−20278.
(51) Xu, J.; Huang, M.; Hu, Z.; Zhang, W.; Li, Y.; Yang, Y.; Zhou, Y.; Zhou, S.; Ma, Z. Prediction and modeling of the basic properties of biomass after torrefaction pretreatment. *J. Anal. Appl. Pyrolysis* **2021**, *159*, 105287.
(52) Ghiasi, M. M.; Mohammadzadeh, O.; Zendehboudi, S. Reliable connectionist tools to determine biodiesel cetane number based on fatty acids methyl esters content. *Energy Convers. Manage.* **2022**, *264*, 115601.
(53) Maheri, M.; Bazan, C.; Zendehboudi, S.; Usefi, H. Machine learning to assess CO_2 adsorption by biomass waste. *J. CO2 Util.* **2023**, *76*, 102590.
(54) Manatura, K.; Chalermsinsuwan, B.; Kaewtrakulchai, N.; Kwon, E. E.; Chen, W.-H. Machine learning and statistical analysis for biomass torrefaction: A review. *Bioresour. Technol.* **2023**, *369*, 128504.
(55) Onsree, T.; Tippayawong, N. Machine learning application to predict yields of solid products from biomass torrefaction. *Renew. Energy* **2021**, *167*, 425−432.
(56) Kartal, F.; Özveren, U. Investigation of the chemical exergy of torrefied biomass from raw biomass by means of machine learning. *Biomass Bioenergy* **2022**, *159*, 106383.
(57) Chen, W.-H.; Aniza, R.; Arpia, A. A.; Lo, H.-J.; Hoang, A. T.; Goodarzi, V.; Gao, J. A comparative analysis of biomass torrefaction severity index prediction from machine learning. *Appl. Energy* **2022**, *324*, 119689.
(58) García Nieto, P. J.; García-Gonzalo, E.; Paredes-Sánchez, J. P.; Bernardo Sánchez, A.; Menéndez Fernández, M. Predictive modelling of the higher heating value in biomass torrefaction for the energy treatment process using machine-learning techniques. *Neural Comput. Appl.* **2019**, *31*, 8823−8836.
(59) Garcia Nieto, P.J.; Garcia−Gonzalo, E.; Sanchez Lasheras, F.; Paredes−Sanchez, J.P.; Riesgo Fernandez, P. Forecast of the higher heating value in biomass torrefaction by means of machine learning techniques. *J. Comput. Appl. Math.* **2019**, *357*, 284−301.
(60) Liu, X.; Yang, H.; Yang, J.; Liu, F. Prediction of fuel properties of torrefied biomass based on back propagation neural network hybridized with genetic algorithm optimization. *Energies* **2023**, *16* (3), 1483.
(61) Kartal, F.; Özveren, U. Prediction of torrefied biomass properties from raw biomass. *Renew. Energy* **2022**, *182*, 578−591.
(62) Onsree, T.; Tippayawong, N.; Phithakkitnukoon, S.; Lauterbach, J. Interpretable machine-learning model with a collaborative game approach to predict yields and higher heating value of torrefied biomass. *Energy* **2022**, *249*, 123676.
(63) Chen, W.-H.; Lo, H.-J.; Aniza, R.; Lin, B.-J.; Park, Y.-K.; Kwon, E. E.; Sheen, H.-K.; Grafilo, L. A. D. R. Forecast of glucose production from biomass wet torrefaction using statistical approach along with multivariate adaptive regression splines, neural network and decision tree. *Appl. Energy* **2022**, *324*, 119775.
(64) Liu, X.; Yang, H.; Yang, J.; Liu, F. Application of random forest model integrated with feature reduction for biomass torrefaction. *Sustainability* **2022**, *14* (23), 16055.
(65) Chen, W.-H.; Lin, B.-J.; Lin, Y.-Y.; Chu, Y.-S.; Ubando, A. T.; Show, P. L.; Ong, H. C.; Chang, J.-S.; Ho, S.-H.; Culaba, A. B. Progress in biomass torrefaction: Principles, applications and challenges. *Prog. Energy Combust. Sci.* **2021**, *82*, 100887.
(66) Brighenti, M.; Grigiante, M.; Antolini, D.; Di Maggio, R. An innovative kinetic model dedicated to mild degradation (torrefaction) of biomasses. *Appl. Energy* **2017**, *206*, 475−486.
(67) Thengane, S. K.; Kung, K. S.; Gomez-Barea, A.; Ghoniem, A. F. Advances in biomass torrefaction: Parameters, models, reactors, applications, deployment, and market. *Prog. Energy Combust. Sci.* **2022**, *93*, 101040.
(68) Agar, D.; DeMartini, N.; Hupa, M. Influence of elevated pressure on the torrefaction of wood. *Energy Fuel.* **2016**, *30* (3), 2127−2136.
(69) Matyjewicz, B.; Świechowski, K.; Koziel, J. A.; Białowiec, A. Proof-of-Concept of high-pressure torrefaction for improvement of pelletized biomass fuel properties and process cost reduction. *Energies* **2020**, *13* (18), 4790.
(70) Svanberg, M.; Olofsson, I.; Flodén, J.; Nordin, A. Analysing biomass torrefaction supply chain costs. *Bioresour. Technol.* **2013**, *142*, 287−296.
(71) Thrän, D.; Witt, J.; Schaubach, K.; Kiel, J.; Carbo, M.; Maier, J.; Ndibe, C.; Koppejan, J.; Alakangas, E.; Majer, S. Moving torrefaction towards market introduction-Technical improvements and economic-environmental assessment along the overall torrefaction supply chain through the SECTOR project. *Biomass Bioenergy* **2016**, *89*, 184−200.
(72) Mahutga, R. R.; Gent, S. P.; Twedt, M. P. Developing a model to predict the torrefaction of biomass. *ASME 2014 8th International Conference on Energy Sustainability collocated with the ASME 2014 12th International Conference on Fuel Cell Science, Engineering and Technology*, Massachusetts, USA, 2014; pp V002T004A002.
(73) Hasan, M.; Haseli, Y. Optimization of a biomass torrefaction plant with near zero emissions. *ASME 2019 13th International Conference on Energy Sustainability collocated with the ASME 2019 Heat Transfer Summer Conference*, Washington, USA, 2019; pp V001T011A007.
(74) Eseyin, A. E.; Steele, P. H.; Pittman, C. U., Jr Current trends in the production and applications of torrefied wood/biomass-A review. *BioResources* **2015**, *10* (4), 8812−8858.
(75) Soh, M.; Phang, F. J. F.; Chai, Y. H.; Chew, J. J.; Loh, S. K.; Yusup, S.; Yu, A.; Sunarso, J. Reaction mechanisms of the wet

https://doi.org/10.1021/acsomega.4c06610
ACS Omega 2025, 10, 6470−6501

torrefaction of oil palm trunks under the effect of initial pressurisation. *Chem. Eng. Res. Des.* **2023**, *193*, 493−506.
(76) Bach, Q.-V.; Tran, K.-Q.; Khalil, R. A.; Skreiberg, Ø.; Seisenbaeva, G. Comparative assessment of wet torrefaction. *Energy Fuel.* **2013**, *27* (11), 6743−6753.
(77) Gao, P.; Liu, Y.; Huang, X.; Abulaiti, A.; Yang, S. Effect of wet torrefaction on the physicochemical characteristics and gasification behavior of biochar. *Ind. Crop. Prod.* **2023**, *197*, 116544.
(78) Moiceanu, G.; Paraschiv, G.; Voicu, G.; Dinca, M.; Negoita, O.; Chitoiu, M.; Tudor, P. Energy consumption at size reduction of lignocellulose biomass for bioenergy. *Sustainability* **2019**, *11* (9), 2477.
(79) Dobbelaere, M. R.; Plehiers, P. P.; Van de Vijver, R.; Stevens, C. V.; Van Geem, K. M. Machine learning in chemical engineering: strengths, weaknesses, opportunities, and threats. *Engineering* **2021**, *7* (9), 1201−1211.
(80) Zendehboudi, S.; Rezaei, N.; Lohi, A. Applications of hybrid models in chemical, petroleum, and energy systems: A systematic review. *Appl. Energy* **2018**, *228*, 2539−2566.
(81) Thon, C.; Finke, B.; Kwade, A.; Schilde, C. Artificial intelligence in process engineering. *Adv. Intell. Syst.* **2021**, *3* (6), 2000261.
(82) khan, M.; Raza Naqvi, S.; Ullah, Z.; Ali Ammar Taqvi, S.; Nouman Aslam Khan, M.; Farooq, W.; Taqi Mehran, M.; Juchelkova, D.; Stepanec, L. Applications of machine learning in thermochemical conversion of biomass-A review. *Fuel* **2023**, *332*, 126055.
(83) Schweidtmann, A. M.; Zhang, D.; von Stosch, M. A review and perspective on hybrid modelling methodologies. *Digt. Chem. Eng.* **2024**, *10*, 100136.
(84) Gu, Y.; Li, B.; Meng, Q. Hybrid interpretable predictive machine learning model for air pollution prediction. *Neurocomputing* **2022**, *468*, 123−136.
(85) Chen, X.-L.; Fu, J.-P.; Yao, J.; Gan, J. Prediction of shear strength for squat RC walls using a hybrid ANN-PSO model. *Eng. Comput.* **2018**, *34*, 367−383.
(86) Zhou, Y. The overall framework design of automatic logistics system using a hybrid ANN-PSO model. *Eng. Comput.* **2022**, *38* (Suppl 3), 2515−2531.
(87) Nourani, V.; Komasi, M. A geomorphology-based ANFIS model for multi-station modeling of rainfall-runoff process. *J. Hydrol.* **2013**, *490*, 41−55.
(88) Rezakazemi, M.; Dashti, A.; Asghari, M.; Shirazian, S. H_2-selective mixed matrix membranes modeling using ANFIS, PSO-ANFIS, GA-ANFIS. *Int. J. Hydrogen Energy* **2017**, *42* (22), 15211−15225.
(89) Barati-Harooni, A.; Najafi-Marghmaleki, A.; Arabloo, M.; Mohammadi, A. H. An accurate CSA-LSSVM model for estimation of densities of ionic liquids. *J. Mol. Liq.* **2016**, *224*, 954−964.
(90) Dai, J.; Chen, N.; Luo, B.; Gui, W.; Yang, C. Multi-scale local LSSVM based spatiotemporal modeling and optimal control for the goethite process. *Neurocomputing* **2020**, *385*, 88−99.
(91) Taghvaei, H.; Amooie, M. A.; Hemmati-Sarapardeh, A.; Taghvaei, H. A comprehensive study of phase equilibria in binary mixtures of carbon dioxide+ alcohols: Application of a hybrid intelligent model (CSA-LSSVM). *J. Mol. Liq.* **2016**, *224*, 745−756.
(92) Yang, L.; Deng, S.; Ma, S.; Xiao, F. Estimation model of leaf nitrogen content based on GEP and leaf spectral reflectance. *Comput. Electr. Eng.* **2022**, *98*, 107648.
(93) Yeddula, B. S. R.; Karthiyaini, S. Experimental investigations and GEP modelling of compressive strength of ferrosialate based geopolymer mortars. *Constr. Build. Mater.* **2020**, *236*, 117602.
(94) Tamanna, A.; Shamsaei, E.; Urquhart, R.; Nguyen, H. D.; Sagoe-Crentsil, K.; Duan, W. Artificial intelligence-based gene expression programming (GEP) model for assessing sprayed seal performance. *Road Mater. Pavement Des.* **2023**, *24* (8), 1977−1994.
(95) Shah, U. A hybrid approach of ANN with PSO for classification problems. *TENCON 2018−2018 IEEE Region 10 Conference*, South Korea, 2018; pp 0611−0616.
(96) Seifi, A.; Ehteram, M.; Singh, V. P.; Mosavi, A. Modeling and uncertainty analysis of groundwater level using six evolutionary optimization algorithms hybridized with ANFIS, SVM, and ANN. *Sustainability* **2020**, *12* (10), 4023.
(97) Finamore, A. R.; Calderaro, V.; Galdi, V.; Graber, G.; Ippolito, L.; Conio, G. Improving wind power generation forecasts: A hybrid ANN-Clustering-PSO approach. *Energies* **2023**, *16* (22), 7522.
(98) Oun, A.; Hazari, N. A.; Niamat, M. Y. Analysis of swarm intelligence based ann algorithms for attacking PUFs. *IEEE Access* **2021**, *9*, 121743−121758.
(99) Gad, A. G. Particle swarm optimization algorithm and its applications: a systematic review. *Arch. Comput. Methods Eng.* **2022**, *29* (5), 2531−2561.
(100) Shafaie, M.; Khademi, M.; Sarparast, M.; Zhang, H. Modified GTN parameters calibration in additive manufacturing of Ti-6Al-4 V alloy: a hybrid ANN-PSO approach. *Int. J. Adv. Manuf. Technol.* **2022**, *123* (11), 4385−4398.
(101) Eberhart, R. C.; Shi, Y.; Kennedy, J. *Swarm Intelligence (Morgan Kaufmann Series in Evolutionary Computation)*, 1st ed.; Morgan Kaufmann Publishers: 2001.
(102) Pant, P.; Chatterjee, D. Prediction of clad characteristics using ANN and combined PSO-ANN algorithms in laser metal deposition process. *Surf. Interfaces* **2020**, *21*, 100699.
(103) Ateş, K. T. Estimation of short-term power of wind turbines using artificial neural network (ANN) and swarm intelligence. *Sustainability* **2023**, *15* (18), 13572.
(104) Aslam, M. N.; Shaheen, A.; Riaz, A.; Alshaikey, S.; Shaukat, N.; Aslam, M. W.; Muhammad, T. An ANN-PSO approach for mixed convection flow in an inclined tube with ciliary motion of Jeffrey six constant fluid. *Case Stud. Therm. Eng.* **2023**, *52*, 103740.
(105) Daneshfar, R.; Bemani, A.; Hadipoor, M.; Sharifpur, M.; Ali, H. M.; Mahariq, I.; Abdeljawad, T. Estimating the heat capacity of non-Newtonian ionanofluid systems using ANN, ANFIS, and SGB tree algorithms. *Appl. Sci.* **2020**, *10* (18), 6432.
(106) Davar, S.; Nobahar, M.; Khan, M. S.; Amini, F. The development of PSO-ANN and BOA-ANN models for predicting matric suction in expansive clay soil. *Mathematics* **2022**, *10* (16), 2825.
(107) Azarpour, A.; Zendehboudi, S. Hybrid smart strategies to predict amine thermal degradation in industrial CO_2 capture processes. *ACS Omega* **2023**, *8* (30), 26850−26870.
(108) Zendehboudi, S.; Ahmadi, M. A.; James, L.; Chatzis, I. Prediction of condensate-to-gas ratio for retrograde gas condensate reservoirs using artificial neural network with particle swarm optimization. *Energy Fuel.* **2012**, *26* (6), 3432−3447.
(109) Babanezhad, M.; Rezakazemi, M.; Marjani, A.; Shirazian, S. Predicting air superficial velocity of two-phase reactors using ANFIS and CFD. *ACS Omega* **2021**, *6* (1), 239−252.
(110) Arya Azar, N.; Ghordoyee Milan, S.; Kayhomayoon, Z. The prediction of longitudinal dispersion coefficient in natural streams using LS-SVM and ANFIS optimized by Harris hawk optimization algorithm. *J. Contam. Hydrol.* **2021**, *240*, 103781.
(111) Ghiasi, M. M.; Mohammadi, A. H.; Zendehboudi, S. Use of hybrid-ANFIS and ensemble methods to calculate minimum miscibility pressure of CO_2-reservoir oil system in miscible flooding process. *J. Mol. Liq.* **2021**, *331*, 115369.
(112) Mousazadeh, F.; Naeem, M. H. T.; Daneshfar, R.; Soulgani, B. S.; Naseri, M. Predicting the condensate viscosity near the wellbore by ELM and ANFIS-PSO strategies. *J. Petrol. Sci. Sci.* **2021**, *204*, 108708.
(113) Jong, C. Y.; Mittal, A.; Tristan, G.; Noller, V.; Chan, H. L.; Goh, Y.; Yeap, E. W. Q.; Dubbaka, S. R.; Nagesh, H. R.; Wong, S. Y. ANFIS-driven machine learning automated platform for cooling crystallization process development. *Org. Process Res. Dev.* **2024**, *28* (4), 1129−1144.
(114) Salleh, M. N. M.; Talpur, N.; Hussain, K. Adaptive neuro-fuzzy inference system: Overview, strengths, limitations, and solutions. *Data Mining and Big Data (DMBB): Second International Conference*, Fukuoka, Japan, 2017; pp 527−535.

https://doi.org/10.1021/acsomega.4c06610
ACS Omega 2025, 10, 6470−6501

(115) Fu, Z.; Cheng, J.; Yang, M.; Batista, J.; Jiang, Y. Wastewater discharge quality prediction using stratified sampling and wavelet denoising ANFIS model. *Comput. Electr. Eng.* **2020**, *85*, 106701.
(116) Mohammadzadeh S, D.; Kazemi, S.-F.; Mosavi, A.; Nasseralshariati, E.; Tah, J. H. M. Prediction of compression index of fine-grained soils using a gene expression programming model. *Infrastructures* **2019**, *4* (2), 26.
(117) Rostami, S.; Rashidi, F.; Safari, H. Prediction of oil-water relative permeability in sandstone and carbonate reservoir rocks using the CSA-LSSVM algorithm. *J. Petrol. Sci. Sci.* **2019**, *173*, 170−186.
(118) Miah, M. I.; Ahmed, S.; Zendehboudi, S.; Butt, S. Machine learning approach to model rock strength: prediction and variable selection with aid of log data. *Rock Mech. Rock Eng.* **2020**, *53*, 4691−4715.
(119) Chen, H.; Duan, J.; Yin, R.; Ponkratov, V. V.; Guerrero, J. W. G. Prediction of penetration rate by coupled simulated annealing-least square support vector machine (CSA-LSSVM) learning in a hydrocarbon formation based on drilling parameters. *Energy Rep.* **2021**, *7*, 3971−3978.
(120) Kamari, A.; Bahadori, A.; Mohammadi, A. H.; Zendehboudi, S. Evaluating the unloading gradient pressure in continuous gas-lift systems during petroleum production operations. *Pet. Sci. Technol.* **2014**, *32* (24), 2961−2968.
(121) Seyyedattar, M.; Zendehboudi, S.; Butt, S. Relative permeability modeling using extra trees, ANFIS, and hybrid LSSVM-CSA methods. *Nat. Resour. Res.* **2022**, *31* (1), 571−600.
(122) Xu, H.; Hassani, V.; Soares, C. G. Truncated least square support vector machine for parameter estimation of a nonlinear manoeuvring model based on PMM tests. *Appl. Ocean Res.* **2020**, *97*, 102076.
(123) Lu, X.; Liu, W.; Zhou, C.; Huang, M. Robust least-squares support vector machine with minimization of mean and variance of modeling error. *IEEE Trans. Neural Netw. Learn. Syst.* **2018**, *29* (7), 2909−2920.
(124) Suykens, J. A.; Vandewalle, J. Least squares support vector machine classifiers. *Neural Process. Lett.* **1999**, *9*, 293−300.
(125) Kamari, A.; Mohammadi, A. H.; Bahadori, A.; Zendehboudi, S. Prediction of air specific heat ratios at elevated pressures using a novel modeling approach. *Chem. Eng. Technol.* **2014**, *37* (12), 2047−2055.
(126) Chamkalani, A.; Zendehboudi, S.; Bahadori, A.; Kharrat, R.; Chamkalani, R.; James, L.; Chatzis, I. Integration of LSSVM technique with PSO to determine asphaltene deposition. *J. Petrol. Sci. Sci.* **2014**, *124*, 243−253.
(127) Seyyedattar, M.; Ghiasi, M. M.; Zendehboudi, S.; Butt, S. Determination of bubble point pressure and oil formation volume factor: Extra trees compared with LSSVM-CSA hybrid and ANFIS models. *Fuel* **2020**, *269*, 116834.
(128) Safari, H.; Shokrollahi, A.; Jamialahmadi, M.; Ghazanfari, M. H.; Bahadori, A.; Zendehboudi, S. Prediction of the aqueous solubility of $BaSO_4$ using pitzer ion interaction model and LSSVM algorithm. *Fluid Phase Equilib.* **2014**, *374*, 48−62.
(129) Holakoei, H. R.; Sajedi, F. Compressive strength prediction of SLWC using RBFNN and LSSVM approaches. *Neural Comput. Appl.* **2023**, *35* (9), 6685−6697.
(130) Metropolis, N.; Rosenbluth, A. W.; Rosenbluth, M. N.; Teller, A. H.; Teller, E. Equation of state calculations by fast computing machines. *J. Chem. Phys.* **1953**, *21* (6), 1087−1092.
(131) Kirkpatrick, S.; Gelatt, C. D., Jr; Vecchi, M. P. Optimization by simulated annealing. *Science* **1983**, *220* (4598), 671−680.
(132) Xavier-de-Souza, S.; Suykens, J. A.; Vandewalle, J.; Bollé, D. Coupled simulated annealing. *IEEE Trans. Syst. Man. Cybern. B Cybern.* **2010**, *40* (2), 320−335.
(133) Chamkalani, A.; Chamkalani, R.; Mohammadi, A. H. Hybrid of two heuristic optimizations with LSSVM to predict refractive index as asphaltene stability identifier. *J. Dispersion Sci. Technol.* **2014**, *35* (8), 1041−1050.
(134) Afzali, S.; Mohamadi-Baghmolaei, M.; Zendehboudi, S. Application of gene expression programming (GEP) in modeling hydrocarbon recovery in WAG injection process. *Energies* **2021**, *14* (21), 7131.
(135) Khan, K.; Jalal, F. E.; Iqbal, M.; Khan, M. I.; Amin, M. N.; Al-Faiad, M. A. Predictive modeling of compression strength of waste pet/scm blended cementitious grout using gene expression programming. *Materials* **2022**, *15* (9), 3077.
(136) Beetham, S.; Capecelatro, J. Multiphase turbulence modeling using sparse regression and gene expression programming. *Nucl. Technol.* **2023**, *209* (12), 1977−1986.
(137) Rezaei, F.; Jafari, S.; Hemmati-Sarapardeh, A.; Mohammadi, A. H. Modeling viscosity of methane, nitrogen, and hydrocarbon gas mixtures at ultra-high pressures and temperatures using group method of data handling and gene expression programming techniques. *Chin. J. Chem. Eng.* **2021**, *32*, 431−445.
(138) Solgi, A.; Pourhaghi, A.; Bahmani, R.; Zarei, H. Pre-processing data using wavelet transform and PCA based on support vector regression and gene expression programming for river flow simulation. *J. Earth Syst. Sci.* **2017**, *126*, 1−17.
(139) Ferreira, C. Gene expression programming: a new adaptive algorithm for solving problems. *Complex Syst.* **2001**, *13* (2), 87−129.
(140) Bagdatli, M. E. C. Vehicle delay modeling at signalized intersections with gene-expression programming. *J. Transp. Eng. A* **2020**, *146* (9), 04020107.
(141) Chen, L.; Wang, Z.; Khan, A. A.; Khan, M.; Javed, M. F.; Alaskar, A.; Eldin, S. M. Development of predictive models for sustainable concrete via genetic programming-based algorithms. *J. Mater. Res. Technol.* **2023**, *24*, 6391−6410.
(142) Pham, V.-N.; Oh, E.; Ong, D. E. Gene-expression programming-based model for estimating the compressive strength of cement-fly ash stabilized soil and parametric study. *Infrastructures* **2021**, *6* (12), 181.
(143) Shabani, S.; Candelieri, A.; Archetti, F.; Naser, G. Gene expression programming coupled with unsupervised learning: a two-stage learning process in multi-scale, short-term water demand forecasts. *Water* **2018**, *10* (2), 142.
(144) Olalusi, O. B.; Durgapershad, A.; Awoyera, P. O.; Kolawole, J. T. Modelling the edge breakout shear capacity of single anchors using gene expression programming. *Neural Comput. Appl.* **2022**, *34* (12), 9635−9646.
(145) Mahmoodzadeh, A.; Alanazi, A.; Hussein Mohammed, A.; Babeker Elhag, A.; Alqahtani, A.; Alsubai, S. An optimized model based on the gene expression programming method to estimate safety factor of rock slopes. *Nat. Hazards* **2024**, *120* (2), 1665−1688.
(146) Ilie, I.; Dittrich, P.; Carvalhais, N.; Jung, M.; Heinemeyer, A.; Migliavacca, M.; Morison, J. I.; Sippel, S.; Subke, J.-A.; Wilkinson, M. Reverse engineering model structures for soil and ecosystem respiration: The potential of gene expression programming. *Geosci. Model Dev.* **2017**, *10* (9), 3519−3545.
(147) Sadeghi, K.; Ghazaie, S. H.; Kalanke, N.; Sokolova, E.; Aghaie, M.; Naserbegi, A.; Modestov, V. Developing reference-based correlations for temperature distribution in VVER reactor using gene expression programming and single-heated channel approach. *Nucl. Eng. Des.* **2024**, *424*, 113233.
(148) Ghazaie, S. H.; Sadeghi, K.; Sokolova, E.; Sergeev, V. Application of gene expression programming in developing correlations for nuclear desalination economic analysis. *Desalination* **2023**, *555*, 116548.
(149) Sadeghi, K.; Ghazaie, S. H.; Sokolova, E.; Cammi, A.; Arab, H. R.; Usta, S. A set of transient correlations for fast and unprotected loss of flow accident in VVER-1000 reactor using single-heated channel approach and Gene Expression Programming. *Ann. Nucl. Energy* **2023**, *183*, 109650.
(150) Li, M.-F.; Li, X.; Bian, J.; Chen, C.-Z.; Yu, Y.-T.; Sun, R.-C. Effect of temperature and holding time on bamboo torrefaction. *Biomass Bioenergy* **2015**, *83*, 366−372.
(151) Onsree, T.; Tippayawong, N. Torrefaction of maize residue pellets with dry flue gas. *BioEnergy Res.* **2020**, *13* (1), 358−368.

https://doi.org/10.1021/acsomega.4c06610
ACS Omega 2025, 10, 6470−6501

(152) Valdez, E.; Tabil, L. G.; Mupondwa, E.; Cree, D.; Moazed, H. Microwave torrefaction of oat hull: Effect of temperature and residence time. *Energies* **2021**, *14* (14), 4298.
(153) Wulandari, W.; Jahsy, N. A.; Tandias, A. H.; Rizkiana, J.; Rubani, I. S.; Saputera, W. H.; Sasongko, D. Torrefaction of rubberwood waste: the effects of particle size, temperature & residence time. *J. Eng. Technol. Sci.* **2020**, *52* (2), 137−152.
(154) Strandberg, M.; Olofsson, I.; Pommer, L.; Wiklund-Lindström, S.; Åberg, K.; Nordin, A. Effects of temperature and residence time on continuous torrefaction of spruce wood. *Fuel Process. Technol.* **2015**, *134*, 387−398.
(155) Bach, Q.-V.; Tran, K.-Q.; Skreiberg, Ø.; Khalil, R. A. Effects of CO_2 on wet torrefaction of biomass. *Energy Procedia* **2014**, *61*, 1200−1203.
(156) Li, R.; Wu, C.; Zhu, L.; Hu, Z.; Xu, J.; Yang, Y.; Yang, F.; Ma, Z. Regulation of the elemental distribution in biomass by the torrefaction pretreatment using different atmospheres and its influence on the subsequent pyrolysis behaviors. *Fuel Process. Technol.* **2021**, *222*, 106983.
(157) Sarvaramini, A.; Larachi, F. Integrated biomass torrefaction-Chemical looping combustion as a method to recover torrefaction volatiles energy. *Fuel* **2014**, *116*, 158−167.
(158) Nguyen, Q.; Nguyen, D. D.; He, C.; Bach, Q.-V. Pretreatment of Korean pine (Pinus koraiensis) via wet torrefaction in inert and oxidative atmospheres. *Fuel* **2021**, *291*, 119616.
(159) Zhao, Z.; Feng, S.; Zhao, Y.; Wang, Z.; Ma, J.; Xu, L.; Yang, J.; Shen, B. Investigation on the fuel quality and hydrophobicity of upgraded rice husk derived from various inert and oxidative torrefaction conditions. *Renew. Energy* **2022**, *189*, 1234−1248.
(160) Hernández, A. B.; Okonta, F.; Freeman, N. Sewage sludge charcoal production by N_2-and CO_2-torrefaction. *J. Environ. Chem. Eng.* **2017**, *5* (5), 4406−4414.
(161) Zhu, X.; Li, S.; Wang, Y.; Zhou, S.; Li, J.; Su, H.; Sun, Y.; Yan, B.; Chen, G. Effect of torrefaction atmospheres on the pyrolysis and combustion of torrefied municipal solid waste. *Fuel* **2024**, *364*, 131056.
(162) Tran, K.-Q.; Trinh, T. N.; Bach, Q.-V. Development of a biomass torrefaction process integrated with oxy-fuel combustion. *Bioresour. Technol.* **2016**, *199*, 408−413.
(163) Torres Ramos, R.; Valdez Salas, B.; Montero Alpírez, G.; Coronado Ortega, M. A.; Curiel Álvarez, M. A.; Tzintzun Camacho, O.; Beleño Cabarcas, M. T. Torrefaction under different reaction atmospheres to improve the fuel properties of wheat straw. *Processes* **2023**, *11* (7), 1971.
(164) Felix, C. B.; Chen, W.-H.; Chang, J.-S.; Park, Y.-K.; Saeidi, S.; Kumar, G. Oxidative torrefaction of microalgae Chlorella sorokiniana: Process optimization by central composite design. *Bioresour. Technol.* **2023**, *382*, 129200.
(165) Zheng, Y.; Li, D.; Wang, J.; Chen, Y.; Liu, C.; Lu, Y.; Lin, X.; Lv, B.; Li, J.; Zheng, Z. Ammonia (NH_3)/nitrogen (N_2) torrefaction pretreatment of waste biomass for the production of renewable nitrogen-containing chemicals via catalytic ammonization pyrolysis: Evolution of fuel-N under a N_2/NH_3-rich atmosphere. *J. Energy Inst.* **2022**, *102*, 143−159.
(166) Haseli, Y. Autothermal operation of a biomass torrefaction plant. *ASME 2018 12th International Conference on Energy Sustainability collocated with the ASME 2018 Power Conference and the ASME 2018 Nuclear Forum*, Florida, USA, 2018; pp V001T004A005.
(167) Satpathy, S. K.; Tabil, L. G.; Meda, V.; Naik, S. N.; Prasad, R. Torrefaction of wheat and barley straw after microwave heating. *Fuel* **2014**, *124*, 269−278.
(168) Medic, D.; Darr, M.; Potter, B.; Shah, A. Effect of torrefaction process parameters on biomass feedstock upgrading. *Fuel* **2012**, *91* (1), 147−154.
(169) Sukiran, M. A.; Abnisa, F.; Syafiie, S.; Daud, W. M. A. W.; Nasrin, A. B.; Aziz, A. A.; Loh, S. K. Experimental and modelling study of the torrefaction of empty fruit bunches as a potential fuel for palm oil mill boilers. *Biomass Bioenergy* **2020**, *136*, 105530.
(170) Artiukhina, E.; Grammelis, P. Modeling of biofuel pellets torrefaction in a realistic geometry. *Therm. Sci.* **2016**, *20* (4), 1223−1231.
(171) Van Poucke, R.; Nachenius, R.; Agbo, K. E.; Hensgen, F.; Bühle, L.; Wachendorf, M.; Ok, Y. S.; Tack, F.; Prins, W.; Ronsse, F. Mild hydrothermal conditioning prior to torrefaction and slow pyrolysis of low-value biomass. *Bioresour. Technol.* **2016**, *217*, 104−112.
(172) Liao, L.; Zheng, J.; Zhang, Y.; Li, C.; Yuan, C. Impact of torrefaction on entrained-flow gasification of pine sawdust: an experimental investigation. *Fuel* **2021**, *289*, 119919.
(173) Deng, J.; Wang, G.-j.; Kuang, J.-h.; Zhang, Y.-l.; Luo, Y.-h. Pretreatment of agricultural residues for co-gasification via torrefaction. *J. Anal. Appl. Pyrolysis* **2009**, *86* (2), 331−337.
(174) Backer, M.; Gladen, A. Impact of salt composition and temperature on low-temperature torrefaction of pine in molten nitrate salts. *Energy* **2023**, *263*, 126044.
(175) Kizuka, R.; Ishii, K.; Ochiai, S.; Sato, M.; Yamada, A.; Nishimiya, K. Improvement of biomass fuel properties for rice straw pellets using torrefaction and mixing with wood chips. *Waste Biomass Volari.* **2021**, *12*, 3417−3429.
(176) Conag, A. T.; Villahermosa, J. E. R.; Cabatingan, L. K.; Go, A. W. Energy densification of sugarcane leaves through torrefaction under minimized oxidative atmosphere. *Energy Sustain. Dev.* **2018**, *42*, 160−169.
(177) Lin, Y.-L.; Zheng, N.-Y.; Hsu, C.-H. Torrefaction of fruit peel waste to produce environmentally friendly biofuel. *J. Clean. Prod.* **2021**, *284*, 124676.
(178) Moreira Miquelino Eleto Torres, C.; Oliveira Carneiro, A. d. C.; Cunha Rodrigues, B. V.; Foresti Salgado Bravo, M.; Mudadu Silva, C. Torrefaction of kraft pulp mills sludges. *Sci. Rep.* **2023**, *13* (1), 22247.
(179) Bach, Q.-V.; Tran, K.-Q.; Skreiberg, Ø. Accelerating wet torrefaction rate and ash removal by carbon dioxide addition. *Fuel Process. Technol.* **2015**, *140*, 297−303.
(180) Youn, H. S.; Kim, G. H.; Um, B. H. Comparative analysis of characteristics based on three processes of kenaf solid fuel: Hydrothermal carbonization, torrefaction, and low ash torrefaction. *Korean J. Chem. Eng.* **2024**, *41* (6), 1743−1755.
(181) Hidayat, S.; Fauzan, R. F. S.; Jeong, S.; Chun, D.; Yoo, J.; Kim, S.; Lim, J.; Rhim, Y.; Lee, S.; Choi, H. Use of torrefaction and solvent extraction to produce ash-less biomass as a solid fuel feedstock for co-firing. *Energy Fuel.* **2017**, *31* (6), 6056−6064.
(182) Namkung, H.; Park, J.-H.; Lee, Y.-J.; Song, G.-S.; Choi, J. W.; Park, S.-J.; Kim, S.; Liu, J.; Choi, Y.-C. Performance evaluation of biomass pretreated by demineralization and torrefaction for ash deposition and PM emissions in the combustion experiments. *Fuel* **2021**, *292*, 120379.
(183) Chen, W.-H.; Kuo, P.-C. A study on torrefaction of various biomass materials and its impact on lignocellulosic structure simulated by a thermogravimetry. *Energy* **2010**, *35* (6), 2580−2586.
(184) Wei, X.; Huang, S.; Wu, Y.; Wu, S.; Yang, J. A comprehensive study on torrefaction of penicillin mycelial residues: Analysis of product characteristics and conversion mechanisms of N. *Fuel* **2022**, *330*, 125703.
(185) Bridgeman, T.; Jones, J.; Shield, I.; Williams, P. Torrefaction of reed canary grass, wheat straw and willow to enhance solid fuel qualities and combustion properties. *Fuel* **2008**, *87* (6), 844−856.
(186) Wang, L.; Barta-Rajnai, E.; Skreiberg, Ø.; Khalil, R.; Czégény, Z.; Jakab, E.; Barta, Z.; Grønli, M. Effect of torrefaction on physiochemical characteristics and grindability of stem wood, stump and bark. *Appl. Energy* **2018**, *227*, 137−148.
(187) Chen, D.; Chen, F.; Cen, K.; Cao, X.; Zhang, J.; Zhou, J. Upgrading rice husk via oxidative torrefaction: Characterization of solid, liquid, gaseous products and a comparison with non-oxidative torrefaction. *Fuel* **2020**, *275*, 117936.
(188) Wang, Z.; Xie, K.; Zhu, W.; Zhang, L.; Zhao, Z.; Xu, L.; Yang, J.; Shen, B. Effects of oxygen deficient and flue gas torrefaction on the

https://doi.org/10.1021/acsomega.4c06610
ACS Omega 2025, 10, 6470−6501

surface property and structural feature of typical agriculture waste: Rice husk. *Fuel* **2022**, *327*, 125211.
(189) Pachón-Morales, J.; Colin, J.; Pierre, F.; Puel, F.; Perré, P. Effect of torrefaction intensity on the flow properties of lignocellulosic biomass powders. *Biomass Bioenergy* **2019**, *120*, 301−312.
(190) Medic, D.; Darr, M.; Shah, A.; Rahn, S. The effects of particle size, different corn stover components, and gas residence time on torrefaction of corn stover. *Energies* **2012**, *5* (4), 1199−1214.
(191) Riaz, S.; Al-Abdeli, Y. M.; Oluwoye, I.; Altarawneh, M. Torrefaction of densified woody biomass: The effect of pellet size on thermochemical and thermophysical characteristics. *BioEnergy Res.* **2022**, *15*, 544−558.
(192) Shang, L.; Nielsen, N. P. K.; Dahl, J.; Stelte, W.; Ahrenfeldt, J.; Holm, J. K.; Thomsen, T.; Henriksen, U. B. Quality effects caused by torrefaction of pellets made from Scots pine. *Fuel Process. Technol.* **2012**, *101*, 23−28.
(193) Tapasvi, D.; Khalil, R.; Skreiberg, Ø.; Tran, K.-Q.; Grønli, M. Torrefaction of Norwegian birch and spruce: an experimental study using macro-TGA. *Energy Fuel.* **2012**, *26* (8), 5232−5240.
(194) Chen, H.; Chen, X.; Qiao, Z.; Liu, H. Release and transformation characteristics of K and Cl during straw torrefaction and mild pyrolysis. *Fuel* **2016**, *167*, 31−39.
(195) Peng, J.; Bi, H.; Sokhansanj, S.; Lim, J. A study of particle size effect on biomass torrefaction and densification. *Energy Fuel.* **2012**, *26* (6), 3826−3839.
(196) Mohamad Aziz, N. A.; Mohamed, H.; Kania, D.; Ong, H. C.; Zainal, B. S.; Junoh, H.; Ker, P. J.; Silitonga, A.S. Bioenergy production by integrated microwave-assisted torrefaction and pyrolysis. *Renew. Sustain. Energy Rev.* **2024**, *191*, 114097.
(197) Grigiante, M.; Antolini, D. Mass yield as guide parameter of the torrefaction process. An experimental study of the solid fuel properties referred to two types of biomass. *Fuel* **2015**, *153*, 499−509.
(198) Kostyniuk, A.; Likozar, B. Catalytic wet torrefaction of biomass waste into bio-ethanol, levulinic acid, and high quality solid fuel. *Chem. Eng. J.* **2024**, *485*, 149779.
(199) Lacombe, E.; Grateau, M.; Marchand, M.; Melkior, T.; Dupont, C. Torrefaction of oak and olive stones in a semi-industrial multiple hearth furnace: Products yields and composition. *Biomass Bioenergy* **2024**, *181*, 107057.
(200) Saleh, S. B.; Hansen, B. B.; Jensen, P. A.; Dam-Johansen, K. Influence of biomass chemical properties on torrefaction characteristics. *Energy Fuel.* **2013**, *27* (12), 7541−7548.
(201) Sarvaramini, A.; Gravel, O.; Larachi, F. Torrefaction of ionic-liquid impregnated lignocellulosic biomass and its comparison to dry torrefaction. *Fuel* **2013**, *103*, 814−826.
(202) Iroba, K. L.; Baik, O.-D.; Tabil, L. G. Torrefaction of biomass from municipal solid waste fractions I: Temperature profiles, moisture content, energy consumption, mass yield, and thermochemical properties. *Biomass Bioenergy* **2017**, *105*, 320−330.
(203) Tanaka, T.; Nambu, I.; Maruyama, Y.; Wada, Y. Sliding-window normalization to improve the performance of machine-learning models for real-time motion prediction using electromyography. *Sensors* **2022**, *22* (13), 5005.
(204) Zhang, X.; Lee, J.; Goh, W. W. B. An investigation of how normalisation and local modelling techniques confound machine learning performance in a mental health study. *Heliyon* **2022**, *8* (5), No. e09502.
(205) Huang, Z.; Yu, Q.; Li, G. Online LSSVM model to predict temperatures of furnace system in Chinese Space Station. *J. Instrum.* **2021**, *16* (07), P07005.
(206) Fadzil, M. A. M.; Zabiri, H.; Razali, A. A.; Basar, J.; Syamzari Rafeen, M. Base oil process modelling using machine learning. *Energies* **2021**, *14* (20), 6527.
(207) Johnston, D. B.; Pembleton, K. G.; Huth, N. I.; Deo, R. C. Comparison of machine learning methods emulating process driven crop models. *Environ. Model. Software* **2023**, *162*, 105634.
(208) Laha, D.; Ren, Y.; Suganthan, P. N. Modeling of steelmaking process with effective machine learning techniques. *Expert Syst. Appl.* **2015**, *42* (10), 4687−4696.
(209) Szlęk, J.; Khalid, M. H.; Pacławski, A.; Czub, N.; Mendyk, A. Puzzle out machine learning model-explaining disintegration process in ODTs. *Pharmaceutics* **2022**, *14* (4), 859.
(210) Yadav, A.; Roy, S. M. An artificial neural network-particle swarm optimization (ANN-PSO) approach to predict the aeration efficiency of venturi aeration system. *Smart Agr. Technol.* **2023**, *4*, 100230.
(211) Tofigh, A. A.; Rahimipour, M. R.; Shabani, M. O.; Davami, P. Application of the combined neuro-computing, fuzzy logic and swarm intelligence for optimization of compocast nanocomposites. *J. Compos. Mater.* **2015**, *49* (13), 1653−1663.
(212) Hameed, I. A. Using Gaussian membership functions for improving the reliability and robustness of students' evaluation systems. *Expert Syst. Appl.* **2011**, *38* (6), 7135−7142.
(213) Yang, Y.; Chen, Y.; Wang, Y.; Li, C.; Li, L. Modelling a combined method based on ANFIS and neural network improved by DE algorithm: A case study for short-term electricity demand forecasting. *Appl. Soft Comput.* **2016**, *49*, 663−675.
(214) Tao, H.; Abba, S. I.; Al-Areeq, A. M.; Tangang, F.; Samantaray, S.; Sahoo, A.; Siqueira, H. V.; Maroufpoor, S.; Demir, V.; Bokde, N. D. Hybridized artificial intelligence models with nature-inspired algorithms for river flow modeling: A comprehensive review, assessment, and possible future research directions. *Eng. Appl. Artif. Intell.* **2024**, *129*, 107559.
(215) Seoni, S.; Jahmunah, V.; Salvi, M.; Barua, P. D.; Molinari, F.; Acharya, U. R. Application of uncertainty quantification to artificial intelligence in healthcare: A review of last decade (2013−2023). *Comput. Biol. Med.* **2023**, *165*, 107441.
(216) Wang, J.; Zhang, H.; Hou, P.; Jia, X. A novel prediction model of desulfurization efficiency based on improved FCM-PLS-LSSVM. *Multimed. Tools Appl.* **2023**, *82* (4), 5685−5708.
(217) Ismail, S.; Shabri, A.; Samsudin, R. A hybrid model of self-organizing maps (SOM) and least square support vector machine (LSSVM) for time-series forecasting. *Expert Syst. Appl.* **2011**, *38* (8), 10574−10578.
(218) Dubdub, I.; Al-Yaari, M. Pyrolysis of mixed plastic waste: II. Artificial neural networks prediction and sensitivity analysis. *Appl. Sci.* **2021**, *11* (18), 8456.
(219) Shuai, C.; Deyou, Y.; Weichun, G.; Chuang, L.; Guowei, C.; Lei, K. Global sensitivity analysis of voltage stability in the power system with correlated renewable energy. *Electr. Pow. Syst. Res.* **2021**, *192*, 106916.
(220) Zhang, P. A novel feature selection method based on global sensitivity analysis with application in machine learning-based prediction model. *Appl. Soft Comput.* **2019**, *85*, 105859.
(221) Brown, C.; Zhang, H. Uncertainty quantification and sensitivity analysis with CASL Core Simulator VERA-CS. *Ann. Nucl. Energy* **2016**, *95*, 188−201.
(222) Strand, J. S.; Goldstein, D. B. Global sensitivity analysis for DSMC simulations of hypersonic shocks. *J. Comput. Phys.* **2013**, *246*, 184−206.
(223) Ilyani Akmar, A.B.; Lahmer, T.; Bordas, S.P.A.; Beex, L.A.A.; Rabczuk, T. Uncertainty quantification of dry woven fabrics: A sensitivity analysis on material properties. *Compos. Struct.* **2014**, *116*, 1−17.
(224) Bouchkira, I.; Latifi, A. M.; Khamar, L.; Benjelloun, S. Global sensitivity based estimability analysis for the parameter identification of Pitzer's thermodynamic model. *Reliab. Eng. Syst. Saf.* **2021**, *207*, 107263.
(225) Leolini, L.; Bregaglio, S.; Moriondo, M.; Ramos, M.; Bindi, M.; Ginaldi, F. A model library to simulate grapevine growth and development: Software implementation, sensitivity analysis and field level application. *Eur. J. Agron.* **2018**, *99*, 92−105.
(226) Sánchez-Mora, H.; Ortiz-Villafuerte, J.; Gómez-Torres, A. M.; Queral, C.; Quezada-García, S. Mathematical model of the QUENCH-06 experiment with sensitivity and uncertainty analysis in hydrogen generation. *Int. J. Heat Mass Transfer* **2023**, *200*, 123553.

https://doi.org/10.1021/acsomega.4c06610
ACS Omega 2025, 10, 6470−6501

(227) Park, J.; Meng, J.; Lim, K. H.; Rojas, O. J.; Park, S. Transformation of lignocellulosic biomass during torrefaction. *J. Anal. Appl. Pyrolysis* **2013**, *100*, 199−206.
(228) Lasode, O. A.; Balogun, A. O.; McDonald, A. G. Torrefaction of some Nigerian lignocellulosic resources and decomposition kinetics. *J. Anal. Appl. Pyrolysis* **2014**, *109*, 47−55.
(229) Yan, W.; Hastings, J. T.; Acharjee, T. C.; Coronella, C. J.; Vásquez, V. R. Mass and energy balances of wet torrefaction of lignocellulosic biomass. *Energy Fuel.* **2010**, *24* (9), 4738−4742.
(230) Ivanovski, M.; Urbancl, D.; Petrovič, A.; Stergar, J.; Goričanec, D.; Simonič, M. Improving lignocellulosic and non-lignocellulosic biomass characteristics through torrefaction process. *Appl. Sci.* **2022**, *12* (23), 12210.
(231) Zhang, Y.; Geng, P.; Liu, R. Synergistic combination of biomass torrefaction and co-gasification: Reactivity studies. *Bioresour. Technol.* **2017**, *245*, 225−233.
(232) Ong, H. C.; Yu, K. L.; Chen, W.-H.; Pillejera, M. K.; Bi, X.; Tran, K.-Q.; Pétrissans, A.; Petrissans, M. Variation of lignocellulosic biomass structure from torrefaction: A critical review. *Renew. Sustain. Energy Rev.* **2021**, *152*, 111698.
(233) Zhang, Y.; Chen, F.; Chen, D.; Cen, K.; Zhang, J.; Cao, X. Upgrading of biomass pellets by torrefaction and its influence on the hydrophobicity, mechanical property, and fuel quality. *Biomass Convers. Biorefin.* **2022**, *12*, 2061−2070.
(234) Demirbas, A. Potential applications of renewable energy sources, biomass combustion problems in boiler power systems and combustion related environmental issues. *Prog. Energy Combust. Sci.* **2005**, *31* (2), 171−192.
(235) da Silva, C. M. S.; Carneiro, A. d. C. O.; Vital, B. R.; Figueiró, C. G.; de Freitas Fialho, L.; de Magalhães, M. A.; Carvalho, A. G.; Cândido, W. L. Biomass torrefaction for energy purposes-Definitions and an overview of challenges and opportunities in Brazil. *Renew. Sustain. Energy Rev.* **2018**, *82*, 2426−2432.
(236) Niu, Y.; Lv, Y.; Lei, Y.; Liu, S.; Liang, Y.; Wang, D. Biomass torrefaction: properties, applications, challenges, and economy. *Renew. Sustain. Energy Rev.* **2019**, *115*, 109395.
(237) Cahyanti, M. N.; Doddapaneni, T. R. K. C.; Kikas, T. Biomass torrefaction: An overview on process parameters, economic and environmental aspects and recent advancements. *Bioresour. Technol.* **2020**, *301*, 122737.

https://doi.org/10.1021/acsomega.4c06610
ACS Omega 2025, 10, 6470−6501